Atmos. Chem. Phys., 24, 3197–3215, 2024
https://doi.org/10.5194/acp-24-3197-2024

Atmospheric Chemistry and Physics
Open Access
EGU

Research article

Contribution of brown carbon to light absorption in emissions of European residential biomass combustion appliances

Satish Basnet[1], Anni Hartikainen[1], Aki Virkkula[2], Pasi Yli-Pirilä[1], Miika Kortelainen[1], Heikki Suhonen[1], Laura Kilpeläinen[1], Mika Ihalainen[1], Sampsa Väätäinen[1], Juho Louhisalmi[1], Markus Somero[1], Jarkko Tissari[1], Gert Jakobi[3,4], Ralf Zimmermann[3,4], Antti Kilpeläinen[5], and Olli Sippula[1,6]

[1]Department of Environmental and Biological Sciences, University of Eastern Finland, 70211, Kuopio, Finland
[2]Atmospheric Composition Research, Finnish Meteorological Institute, 00101, Helsinki, Finland
[3]Department of Analytical and Technical Chemistry, University of Rostock, 18059 Rostock, Germany
[4]Joint Mass Spectrometry Centre, Comprehensive Molecular Analytics, Helmholtz Zentrum München, 85764 Neuherberg, Germany
[5]School of Forest Sciences, University of Eastern Finland, 80101, Joensuu, Finland
[6]Department of Chemistry, University of Eastern Finland, 80101, Joensuu, Finland

Correspondence: Satish Basnet (satish.basnet@uef.fi), Anni Hartikainen (anni.hartikainen@uef.fi), and Olli Sippula (olli.sippula@uef.fi)

Received: 3 October 2023 – Discussion started: 13 October 2023
Revised: 4 January 2024 – Accepted: 22 January 2024 – Published: 14 March 2024

Abstract. Residential biomass combustion significantly contributes to light-absorbing carbonaceous aerosols in the atmosphere, impacting the earth's radiative balance at regional and global levels. This study investigates the contribution of brown carbon (BrC) to the total particulate light absorption in the wavelength range of 370–950 nm ($BrC_{370–950}$) and the particulate absorption Ångström exponents ($AAE_{470/950}$) in 15 different European residential combustion appliances using a variety of wood-based fuels. $BrC_{370–950}$ was estimated to be from 1 % to 21 % for wood log stoves and 10 % for a fully automatized residential pellet boiler. Correlations between the ratio of organic to elemental carbon (OC / EC) and $BrC_{370–950}$ indicated that a one-unit increase in OC / EC corresponded to approximately a 14 % increase in $BrC_{370–950}$. Additionally, $BrC_{370–950}$ was clearly influenced by the fuel moisture content and the combustion efficiency, while the effect of the combustion appliance type was less prominent. $AAE_{470/950}$ of wood log combustion aerosols ranged from 1.06 to 1.61. By examining the correlation between $AAE_{470/950}$ and OC / EC, an $AAE_{470/950}$ close to unity was found for pure black carbon (BC) particles originating from residential wood combustion. This supports the common assumption used to differentiate light absorption caused by BC and BrC. Moreover, diesel aerosols exhibited an $AAE_{470/950}$ of 1.02, with BrC contributing only 0.66 % to the total absorption, aligning with the assumption employed in source apportionment. These findings provide important data to assess the BrC from residential wood combustion with different emission characteristics and confirm that BrC can be a major contributor to particulate UV and near-UV light absorption for northern European wood stove emissions with relatively high OC / EC ratios.

Published by Copernicus Publications on behalf of the European Geosciences Union.

1 Introduction

Atmospheric aerosols play a crucial role in various atmospheric processes and have direct and indirect effects on the earth's radiative forcing and energy budget. Among these aerosols, black carbon (BC) is a significant component that contributes to global warming due to its light-absorbing properties (Bond et al., 2013; IPCC, 2014). Here, we determine BC as the optically defined fraction of soot (Petzold et al., 2013). It is primarily emitted into the atmosphere through incomplete combustion of fossil fuels, biofuels, and biomass burning (BB), including activities such as forest fires, residential combustion, engines, and industrial processes (Klimont et al., 2017). In addition to BC, certain fractions of organic aerosols, known as "brown carbon" (BrC), exhibit significant light absorption in the visible and near-UV wavelengths (Kirchstetter et al., 2004), thereby playing a role in radiative forcing (Cappa et al., 2019; Liu et al., 2015). According to numerous studies, low-temperature biomass and biofuel burning, including small-scale residential wood combustion (RWC), are the primary sources of atmospheric BrC (Cappa et al., 2019; Pokhrel et al., 2017; Saleh et al., 2014; Cheng et al., 2011; Z. Li et al., 2019).

RWC is a significant contributor to the energy supply in Europe and many other parts of the world. Unfortunately, RWC's sustainability is hindered by its high emissions of particulate matter (PM) and gases, which have detrimental effects on climate, human health, and the environment. In the European Union (EU), small-scale combustion is recognized as a primary source of particulate pollution, accounting for over 45 % of total fine particulate matter ($PM_{2.5}$) emissions (EEA, 2013). In Finland, RWC is the largest source of BC emission and is estimated to contribute up to 55 % to the total BC emitted (Savolahti et al., 2016). The accurate quantifying of the amount and impacts of the absorbing aerosols emitted from RWC is challenged by the gaps in knowledge regarding the particle optical properties and potential variance in emission factors (EFs). However, only a few RWC appliance types and fuels have been studied (e.g., Fang et al., 2022; Martinsson et al., 2015; Zhang et al., 2020; Saleh et al., 2013; Kumar et al., 2018; Saliba et al., 2018; Olsen et al., 2020; Li et al., 2022; Leskinen et al., 2023; Tissari et al., 2019; Hartikainen et al., 2020; Savolahti et al., 2016, 2019; Sun et al., 2021), which causes uncertainties in assessing the direct radiative forcing of RWC emissions. The inclusion of BrC in emission inventories is further constrained by the lack of characterization and quantification of BrC emissions. Global simulations have indicated that BrC contributes approximately 10 %–50 % of the total absorption by atmospheric aerosols (Feng et al., 2013; Bahadur et al., 2012; Lack et al., 2012). In the case of biomass and wood log combustion, BrC has been found to contribute up to 20 %–90 % of light absorption in fresh RWC emissions at shorter visible wavelengths (Fang et al., 2022; Martinsson et al., 2015). In addition, the optical properties of emissions undergo changes in the atmosphere, which adds further complexity to estimating their climate effects (Laskin et al., 2015; Kumar et al., 2018; Zhong and Jang, 2014; Wang et al., 2019; Lack et al., 2012).

For the quantification of BrC, various optical measurement techniques have been employed (Fang et al., 2022; Pani et al., 2021; Pokhrel et al., 2017; Olson et al., 2015; Martinsson et al., 2015; Bahadur et al., 2012; Zhang et al., 2020; Li et al., 2022; Sun et al., 2021; Zhang et al., 2021; Rathod and Sahu, 2022; Massabò et al., 2015). The methods commonly involve the determination of the wavelength-dependent light absorption and subtracting the inferred BC absorption at specific wavelengths. The wavelength dependence of aerosol light absorption is generally described by the absorption Ångström exponent (AAE; Eq. 1) (Fang et al., 2022; Olson et al., 2015; Bahadur et al., 2012; Martinsson et al., 2015) based on a selected wavelength pair:

$$\mathrm{AAE}_{\lambda_1/\lambda_2} = -\frac{\ln\left(b_{\mathrm{abs},\lambda_1}/b_{\mathrm{abs},\lambda_2}\right)}{\ln\left(\lambda_1/\lambda_2\right)}. \quad (1)$$

BC exhibits strong light absorption across the visible spectrum, which typically results in an AAE of approximately 1.0. Higher AAE values are often assumed to indicate the presence of BrC. However, AAEs in the range of 0.8–1.4 have been measured and modeled even for pure BC particles (Liu et al., 2018; Virkkula, 2021), introducing uncertainty when determining BrC absorption (Lack and Langridge, 2013). Furthermore, the use of aethalometers, common instruments for real-time measurements of BC particles in ambient air, introduces additional uncertainties to BC and BrC quantification. The aethalometer measures the optical attenuation by aerosol particles collected on a filter, and converting the measured infrared light attenuation to the mass concentration of equivalent black carbon (eBC) requires knowledge of the mass absorption cross-section (MAC) of the particles and the multiple scattering factor (C) in the filter (Weingartner et al., 2003; Drinovec et al., 2015; Sandradewi et al., 2008; Virkkula et al., 2007). Typically, the MAC and C predefined by the instrument manufacturer are applied. However, various experiments using alternative instruments in conjunction with an aethalometer have shown higher C values for biomass combustion and ambient air aerosols than those proposed by the instrument manufacturer (Kumar et al., 2018; Tasoglou et al., 2017; Yus-Díez et al., 2021; Backman et al., 2017).

In this study, we define BC and BrC emissions from a range of different northern European wood combustion appliances using wavelength-dependent aerosol absorption data from a seven-wavelength aethalometer and thermal–optical carbon analysis of particle samples. The contribution of BC and BrC to the total light absorption is determined considering both the whole aethalometer wavelength range and the specific wavelengths. We investigate the effects of combustion technologies and fuel properties on the particulate AAE and BrC light absorption. Finally, we correlate particulate

composition and combustion conditions with AAE and BrC absorption, as well as establish parameterizations to evaluate the contribution of BrC to particle light absorption in RWC emissions.

2 Methods

The combustion experiments were performed in two facilities at the University of Eastern Finland using seven different fuels and 15 different combustion appliances in total. Firstly, masonry heater, chimney stove, pellet boiler, and non-road diesel engine experiments were performed at the ILMARI laboratory (http://www.uef.fi/ilmari, last access: 6 March 2024). Secondly, measurements with the masonry heater and 10 types of sauna stoves were conducted at the small-scale combustion simulator (SIMO) (https://sites.uef.fi/fine/front-page/simo/, 6 March 2024; Tissari et al., 2019). The emission sources along with the fuels and details of measurement campaigns are summarized in Table 1. Details of the experimental setups, fuels used, and basic emission characterization have been published elsewhere (see references in Table 1) for all experiments except for a subsection of experiments performed with the pellet boiler and the non-road diesel engine, as well as the modern chimney stove experiments performed in ILMARI in 2021. The following sections briefly explain the experimental setups for emission sources. The fuel compositions are shown in Table S1 in the Supplement and the experimental setups at the ILMARI and SIMO facilities are illustrated in Fig. S1 in the Supplement.

2.1 Combustion appliances and fuels

2.1.1 Modern masonry heater

The modern masonry heater (MMH) (model HIISI; Tulikivi, Juuka, Finland) was used with three different wood species, i.e., beech (*Fagus sylvatica*), birch (*Betula pubescens*), and spruce (*Picea abies*), at the ILMARI facility of the University of Eastern Finland. Each experiment lasted for 4 h with six batches of wood combustion, each burning for approximately 30 min. After the final batch was consumed, the embers were stoked and secondary air channels were closed for residual char combustion measurement. The total amount of wood combusted was approximately 15 kg per experiment ($\sim$ 2.5 kg per batch). The detailed experimental setups and procedures, along with the fuel properties and emission characterization, can be found in Czech et al. (2018) and Kortelainen et al. (2018).

2.1.2 Conventional masonry heater

The Finnish logwood-fired conventional masonry heater (CMH) designed for laboratory studies was used in the SIMO with birch as fuel. Each combustion experiment had three batches, and a total of approximately 4.65 kg ($1.65 + 1.5 + 1.5$ kg) of fuel was burned. The detailed experimental setup, fuel properties, and emission characterization can be found in Suhonen et al. (2021).

2.1.3 Sauna stove

Wood burning in sauna stoves (SS) was extensively measured in the SIMO facility. The typical use of sauna stoves in Finland was simulated using 10 different types of commercially available SS. Three batches of birch were combusted with a total load of approximately 7 kg (3 kg + 3 kg + 1 kg). The differences regarding the 10 SS types, fuel properties, and emission characterization are discussed in detail by Tissari et al. (2019). The major differences regarding the stoves were that SS1–SS4, SS8, and SS9 were traditional steel stoves, SS5 had long flue gas ducts at both sides of the stove, and SS6, SS7, and SS10 had stones covering the stove's outer shell. SS1 and SS8 specifically used fuels with different moisture content, allowing the study of the impact of fuel moisture content on the emissions. The fuel moisture contents used for the experiments were 11 %, 17 % and 18 %, and 28 %. For this work, we have classified the SS results according to the fuel moisture contents, i.e., the results were averaged accordingly as SS-11 with 11 %, SS-18 with 17 % and 18 %, and SS-28 with 28 % fuel moisture content because of the similarity of the optical properties between the SS types when using similar fuel moisture contents.

2.1.4 Modern chimney stove

The modern chimney stove (MCS) (model 9.3; Aduro, Hasselager, Denmark) was used in two different experimental campaigns in the ILMARI facility. In 2016, this non-heat-retaining MCS was used to burn two wood species, i.e., pine (*Pinus sylvestris*) and spruce (*Picea abies*). Every combustion experiment included five batches, each containing approximately 2 kg of wood logs. After the combustion of the final batch, the embers were stoked and emissions were measured from the residual char with the secondary air channel closed. An experiment lasted for 4 h with each batch burning for approximately 35–45 min. Detailed information about the experimental setups, fuel properties, and the characterization of emissions can be found in Ihantola et al. (2020).

The second set of experiments using MCS was conducted in 2021 in the ILMARI facility using beech logs as fuel. Each combustion experiment had six batches with individual batches consisting of approximately 2 kg of wood logs. The embers were stocked after the final batch was consumed and the secondary air channel was closed during the residual char combustion.

The MCS was further used to burn peat briquets in the set of experiments conducted in 2021 in the ILMARI facility. The peat combustion experiment lasted for 4 h, with eight 1 kg batches each burning for approximately 25 min. The first batch of fuel was added to the smoldering embers of beech

Table 1. Appliance types, fuel burned, fuel moisture content, and fuel batch details for the measurement campaigns under investigation.

Appliance	Abbrev.	Measurement site and date	Fuel type	Fuel moisture (%)	Number of repetitions	Number of batches	Time per batch (min)	Average batch size (kg)	Reference
Modern masonry heater	MMH	ILMARI, 2013	Beech	9 %	4	6	30	2.5	Czech et al. (2018),
			Spruce	7.4 %	3	6	30	2.5	Kortelainen et al. (2018),
			Birch	7.2 %	6	6	30	2.5	Leskinen et al. (2014)
Conventional masonry heater	CMH	SIMO, 2019	Birch	11 %	3	3–4	25	1.5	Suhonen et al. (2021)
Sauna stoves (10 types)	SS-11	SIMO, 2018	Birch	11 %	23	3	15–45	3 + 3 + 1	Tissari et al. (2019)
	SS-18		Birch	18 %	12	3	15–45	3 + 3 + 1	
	SS-28		Birch	28 %	3	3	15–45	3 + 3 + 1	
Modern chimney stove	MCS	ILMARI, 2016	Pine	6.1 %	3	5	35–45	2	Ihantola et al. (2020)
			Spruce	7.4 %	3	5	35–45	2	
		ILMARI, 2021	Beech	9 %	14	6	35	2	
			Peat	17.9 %	3	8	25	1	
Pellet boiler	PB	ILMARI, 2016	Softwood Pellets	7.3 %	3	4	60		
Non-road diesel engine	NrDE	ILMARI, 2016	Diesel		3	4	60		

logs to ease the ignition of peat, which led to flaming conditions for the whole peat-burning experiment.

2.1.5 Pellet boiler

A modern small-scale (25 kW) pellet boiler (PB) (model PZ-RL; Biotech Energietechnik, Thalgau, Austria) was used with softwood pellets as fuel in the ILMARI facility. The stove's detailed description can be found in Lamberg et al. (2011a). The PB was operated under four different load capacities: low-load (7 kW), half-load (12.5 kW), high-load (18.5 kW), and full-load capacity (25 kW). The combustion lasted for 4 h, with each mode operating for 1 h before switching to the next load in ascending order.

2.1.6 Non-road diesel engine

A U.S. Environmental Protection Agency tier 1 / European Union stage-II water-cooled, non-road diesel engine (NrDE) (24.5 kW, 3000 rpm, total displacement of 1123 cm^3; model D1105-T; Kubota, Argenteuil, France) was used in the ILMARI facility in 2016. The engine was operated using a four-stage test cycle for which the operating modes were selected based on the C1 test type of the ISO 8178 standard. The operating modes were idle (880 rpm), intermediate 50 % (2050 rpm, 39.92 N m, 8.57 kW), rated 10 % (3000 rpm, 7.07 N m, 2.22 kW), and rated 50 % (3000 rpm, 35.33 N m, 11.10 kW). The load of the engine was controlled with a liquid-cooled eddy current engine dynamometer (model AG-30HS; Froude Cosine, Novi, Michigan, USA) capable of producing a maximum power of 30 kW and a maximum torque of 90 Nm (14 000 rpm). The test fuel was European commercial diesel (EN 590). Each experiment lasted for 4 h, with each cycle operating for 1 h before switching to the next cycle in the above-mentioned order.

2.2 Aerosol measurements

Aerosol light absorption and equivalent black carbon (eBC) mass concentration were measured using a dual-spot aethalometer (model AE33; Magee Scientific, Berkeley, California, USA). The instrument uses two sample spots with different flow rates for aerosol accumulation and an unloaded spot as a reference area for calculating the light absorption coefficients ($b_{abs}(\lambda)$). The instrument measures light attenuation at seven wavelengths (370, 470, 520, 590, 660, 880, and 950 nm). The AE33 automatically compensates for the filter-loading parameter (k) and multiple scattering coefficients (C) in real time (Drinovec et al., 2015, 2017). In experiments prior to 2021, a filter tape made of tetrafluoroethylene-coated glass fibers (M8020) was used for AE33. For this filter tape, a C value of 1.57 and a leakage factor of 0.07 were applied as specified by the manufacturer (Drinovec et al., 2015). For the ILMARI 2021 experiments, a newer filter tape (M8060, made of glass fibers coated with polytetrafluoroethylene or polyethylene terephthalate) with a recommended or assumed C value of 1.39 and a leakage factor of 0.01 was used.

Two aethalometer instruments were used: AE33a in the ILMARI facility and AE33b in the SIMO facility. During the MCS experiments in ILMARI in 2021, the two AE33s were utilized in line to compare the instruments' efficiency and reliability. Low variation between AE33a and AE33b

(0.87 ± 0.09 on average $\pm$ standard deviations of the average values of the four experiments for the whole experiments, and 0.89 ± 0.09 for batch-wise averages excluding the ember phase) was observed in the measured eBC values by both AE33s, validating the reliability of AE33 data. Time series for eBC emission concentration derived simultaneously from the two instruments (AE33a and AE33b) for 2 experimental days are presented in Fig. S2.

The particle number size distributions were measured with an electrical low-pressure impactor (Classic ELPI; Dekati, Kangasala, Finland). Organic carbon (OC) and elemental carbon (EC) were collected on quartz fiber filters (Pallflex Tissuquartz; Pall Corporation, New York, USA) and analyzed with a thermal–optical method (Turpin et al., 2000) using a carbon analyzer (Sunset Laboratory; Tigard, Oregon, USA). The U.S. National Institute for Occupational Safety and Health (NIOSH) protocol 5040 (NIOSH, 1999) was used for all experiments except for ILMARI (in 2021), where the analyses were based on the Interagency Monitoring of Protected Visual Environments (IMPROVE-A) protocol (Chow et al., 2007). Both protocols have been found to reliably provide the OC and EC concentrations (Wu et al., 2016). However, the IMPROVE-A protocol provides slightly more detailed information about OC and EC fractions at different temperatures than the NIOSH 5040 protocol. Furthermore, IMPROVE-A includes a reflectance-based optical correction that enables the analysis of heavily loaded filters.

2.3 Sampling

The raw flue gas sample was directed to the gas analyzers through an insulated and heated (180 °C) sample line with a ceramic filter. In the ILMARI setup, gaseous emissions (CO_2, CO, and NO_x) were measured by ABB Hartman & Braun (ABB Cemas Gas Analysing Rack; ABB Automation, Zurich, Switzerland) and Siemens (ULTRAMAT 23; Siemens, Munich, Germany) gas analyzer systems (Fig. S1). Similarly, the SIMO setup used Siemens ULTRAMAT 23 gas analyzers to measure CO_2, CO, and NO in the undiluted exhaust.

For the particle measurements, the sample was led through a two-stage dilution system. The first stage of dilution was performed with a porous tube diluter where the sample was diluted with clean air of ambient temperature followed by an ejector diluter (ED) (DAS; Venacontra, Kuopio, Finland). In ILMARI, the dilution ratio (DR) after the first two stages of the dilution was 10–100 (Table S2). Additional ED (VKL 10 E; Palas, Karlsruhe, Germany) was used upstream of the aethalometer to further dilute the sample by an additional factor of 100 to reach suitable concentrations for aethalometer measurements. In SIMO, the initial DR after two stages of dilution was $\sim$ 73–90 and an additional ED (DI-1000; Dekati) was used upstream of the aethalometer to dilute the sample by an additional factor of 8.6. The DR was defined from CO_2 concentrations in the raw gas and in the diluted sample (ABB CO_2 analyzer or GMP343 (Vaisala, Vantaa, Finland) in ILMARI or GMP343 in SIMO) as described by Sippula et al. (2009).

2.4 Data analysis

2.4.1 Segregation of black and brown carbon

The contribution of black and brown carbon to the total absorption of visible light was segregated by calculating the "dimensionless integrated absorptions" (DIA) of BC and BrC over the measured wavelength range. This approach relies on the multi-wavelength attenuation measurement and is comparable to the multi-wavelength absorption analyzer model (Massabò et al., 2015; Bernardoni et al., 2017). First, the dimensionless integrated absorption by BC (DIA_{BC}) was calculated by a definite integral of Eq. (2) for the aethalometer wavelength range (370–950 nm) using the absorption coefficient value at the wavelength of 880 nm ($b_{abs}(880\,nm)$), where the light absorption was assumed to be the result of BC. The BC absorption was extrapolated to lower wavelengths assuming that BC had an AAE (AAE_{BC}) of 1:

$$b_{abs,\,BC}(\lambda) = b_{abs}(880\,nm) \times \left(\frac{\lambda}{880}\right)^{-AAE_{BC}}. \quad (2)$$

For the calculation of the total absorption, a power law function was fit to the total aerosol absorption coefficients measured at the seven aethalometer wavelengths using the method of least squares. As a result, we attain an AAE describing the wavelength dependency over the visible wavelength range ($AAE_{370–950}$). The total dimensionless integrated absorption (DIA_{Tot}) was then calculated as the definite integral of this power law function over the aethalometer wavelength range. As the total absorption can be considered to be the sum of the absorptions by BC and BrC, the dimensionless integrated absorption by BrC (DIA_{BrC}) was defined as the difference between the DIA_{Tot} and the DIA_{BC}. The relative contribution of BrC to the total absorption over wavelength 370–950 nm ($BrC_{370–950}$) was calculated as the ratio of DIA_{BrC} to DIA_{Tot}. A step-by-step example of this calculation is shown in Sect. S1 in the Supplement.

The absorptions by BC and BrC were also segregated for the individual wavelengths, for which the absorption by BrC was estimated as the difference between the total absorption and the absorption by BC (Olson et al., 2015). Major uncertainties in the relative contribution by BrC may arise due to the choice of value for AAE_{BC}, which may vary with differences in combustion emission. As the exact AAE for pure BC cannot be obtained with this instrumentation, we used the standard AAE_{BC} of 1.0. Despite the uncertainties associated with this approach (Lack and Langridge, 2013), many studies have found the results in agreement with other methods of apportioning BC and BrC absorption (Tian et al., 2020; Zhang et al., 2019; Briggs and Long, 2016). The sensitivity of $BrC_{370–950}$ to the choice of AAE_{BC} depends on the amount

of BrC, as illustrated in Figs. S14 and S15 for AAE_{BC} values of 0.9 or 1.1 instead of 1.0. The results are, however, presented for an AAE_{BC} of 1.0, with a brief discussion on the effects of AAE_{BC} on the resolved absorption by BrC available in Sect. 3.2.

The eBC mass concentrations were converted from the $b_{abs}(880\,nm)$ by multiplying it with the generally assumed MAC of eBC at 880 nm (MAC_{aeth}, 7.77 $m^2\,g^{-1}$) (Eq. 3):

$$eBC = b_{abs}(880\,nm)/MAC_{aeth}(880\,nm). \quad (3)$$

The actual MACs may diverge from the default MAC_{aeth} with different emission sources (e.g., Olson et al., 2015). To assess the MAC of the emitted BC particles, the $MAC_{880\,nm}$ was estimated by dividing the measured b_{abs} by the thermo-optically derived EC concentration (Eq. 4):

$$MAC_{880\,nm} = \frac{b_{abs}\,(880\,nm)}{EC}. \quad (4)$$

Furthermore, the MAC of the organic fraction (MAC_{OC}) was estimated from the ratio between $b_{abs,\,BrC}(470\,nm)$, and the concentration of OC from the thermal-based method (Eq. 5):

$$MAC_{OC,470\,nm} = \frac{b_{abs,\,BrC}\,(470\,nm)}{OC}. \quad (5)$$

The two-wavelength $AAE_{470/950}$ values typically used for source apportionment of ambient aerosol were calculated using the wavelength pair 470 and 950 nm (Eq. 6) as suggested by Zotter et al. (2017):

$$AAE_{470/950} = \frac{-\ln\left(b_{abs,470\,nm}/b_{abs,950\,nm}\right)}{\ln(470\,nm/950\,nm)}. \quad (6)$$

2.4.2 Emission factors

The emission factors (EFs) were calculated as milligrams of PM (OC, EC, or eBC) per megajoule of energy produced by applying Eq. (7) (Reda et al., 2015):

$$EF = c_n \times \alpha \times k \times Q_s, \quad (7)$$

where c_n is the dilution-corrected concentration (in mg m^{-3}) of species in flue gas. α is the air-to-fuel ratio during the combustion process calculated from either raw flue gas O_2 concentration (ILMARI experiments; Eq. 8) or raw flue gas CO_2 concentration (SIMO experiments; Eq. 9). k is the correction factor for the fuel moisture content given by Eq. (10), where H_u is the net heating value of dry fuel and H_w is the amount of heat consumed in water evaporation which depends on the ratio of water to dry substance in fuel (W_v) and the latent heat of vaporization of water (l_v) (2.50 MJ kg^{-1} at 0 °C; Eq. 11). (The net heating values for the dry fuels used in different experiments are listed in Table S1.) Q_s is the dry volume of flue gas produced in the combustion of dry fuel (0.25 m^3 MJ^{-1} for solid fuels and 0.26 m^3 MJ^{-1} for diesel fuel):

$$\alpha = \frac{20.9\,\%}{20.9\,\% - O_2\,\%} \quad (8)$$

$$\alpha = \frac{20.2\,\%}{CO_2\,\%} \quad (9)$$

$$k = \frac{H_u}{H_u - H_w} \quad (10)$$

$$H_w = W_v \times l_v. \quad (11)$$

The modified combustion efficiency (MCE; Eq. 12) was calculated to define the degree of completeness of a combustion process:

$$MCE = \frac{\Delta CO_2}{(\Delta CO_2 + \Delta CO)}, \quad (12)$$

where ΔCO and ΔCO_2 are the background-corrected CO and CO_2 values in the exhaust.

2.4.3 Data handling and uncertainty estimation

The mean EFs for each fuel–appliance combination were calculated from the experiment-wise means averaged over the whole measurement period. These experiment-wise average EFs were further averaged according to the number of repetitions for each fuel type in individual combustion appliances ($n = 3$–23; Table 1), and results are given as mean EFs ± standard deviations (SD) of the repetition means. The $AAE_{470/950}$ and BrC contributions were calculated from the combustion period averaged $b_{abs}(\lambda)$ coefficient and further averaged according to the number of repetitions. The SD of $AAE_{470/950}$ is given as the mean of standard deviations of the time-resolved data. The SD of $MAC_{880\,nm}$ was calculated from $MAC_{880\,nm}$ values for each fuel type in individual combustion appliances.

The uncertainties related to the $AAE_{470/950}$ and the BrC absorption contribution depend on rates of change and uncertainties related to the attenuation and loading compensation parameters. The uncertainty in $AAE_{470/950}$ was derived as in Helin et al. (2021), and an overview of the estimated average relative uncertainty in $AAE_{470/950}$ over 1 min, individual batches, and the complete combustion experiments is available in Table S3.

A detailed explanation regarding the uncertainty of the BrC absorption contribution is given in Sect. S2. The change in attenuation during each experiment was considered for the complete experiment, except for peat combustion, for which individual batches were considered instead. The absolute uncertainties in the fractions of absorption by BC and BrC are shown in Fig. S4 for individual wavelengths for each fuel–appliance combination. Among RWC, sauna stoves (SS-11 and SS-18) showed the highest amount of absolute uncertainty in BrC absorption with a median value of ∼ 7 % and ∼ 10 %, respectively, for all calculated wavelengths, while MCS showed the least absolute uncertainty (∼ 0.6 %). For

the overall experiments, peat combustion showed the least amount of uncertainty with a median value of 0.01 % BrC contribution (470 nm). However, since the values for peat combustion were calculated from the individual batches, the uncertainty values are not fully comparable to those of the other combustion sources. When considering the experiment-to-experiment variation in the uncertainty of the results, the diesel engine showed the least absolute uncertainty (median uncertainty ~ 0.3 % BrC contribution). However, the relative uncertainties in the contribution of BrC to the absorption were the highest when the BrC contribution was low, namely, for diesel exhaust emissions (0.66 %).

3 Results and discussion

3.1 Emission factors and combustion conditions

The EFs for OC, EC, and eBC (average $\pm$ standard deviation of the experiment-wise means) are presented in Fig. 1. Among wood log combustion appliances, the highest eBC EF was observed for pine combustion in MCS ($80.9 \pm 45.7\,\mathrm{mg\,MJ^{-1}}$), while the lowest was recorded for spruce combustion in MMH ($27.9 \pm 4.41\,\mathrm{mg\,MJ^{-1}}$). Birch combustion in SS-11 ($61.3 \pm 34.4\,\mathrm{mg\,MJ^{-1}}$) and birch combustion in CMH ($59.4 \pm 14.5\,\mathrm{mg\,MJ^{-1}}$) exhibited the highest EFs for EC, whereas the lowest EC EF was found for spruce combustion in MMH ($16.9 \pm 1.23\,\mathrm{mg\,MJ^{-1}}$). Good correlations were observed between EC and eBC concentrations within the fuel–appliance combinations (Fig. S5). However, there was a disparity between the relations of eBC and EC between the different combustion fuel–appliance combinations, suggesting variations in the optical properties of emitted particles as discussed further in Sect. 3.2.

The lowest OC EFs were observed for MMH, regardless of the wood species used. The formation of OC was influenced by fuel moisture, with the highest OC EF observed for high moisture content fuel combustion in SS-28 ($51.8 \pm 10.0\,\mathrm{mg\,MJ^{-1}}$). Increased fuel moisture content decreases the temperature during RWC, which leads to increased emissions of particulate organic matter (Price-Allison et al., 2021, 2019; Magnone et al., 2016). The OC / EC ratio in the exhaust from sauna stoves increased from 0.51 ± 0.42 for 11 % moisture content to 1.49 ± 0.16 for 28 % moisture content. A moderate correlation was observed ($R^2 = 0.67$) between the OC / EC ratio and fuel moisture content for the wood log fuel–appliance-wise averaged combination (Fig. S6a). The presented EFs for EC, eBC, and OC from logwood appliances primarily represent typical northern European wood stoves and generally align with similar studies conducted in Europe (Savolahti et al., 2016; Vicente and Alves, 2018) and North America (Tasoglou et al., 2017). In comparison with wood log combustion, pellet burning exhibited significantly lower EFs for OC, EC, and eBC (1.01 ± 0.25, 7.08 ± 3.29, and $8.03 \pm 1.62\,\mathrm{mg\,MJ^{-1}}$, respectively), supporting previous findings that pellet burners are relatively clean appliances (Lamberg et al., 2011a, b).

The particle number size distributions resulting from wood log combustion were generally characterized by a single dominant mode, with aerodynamic geometric mean diameters (GMDs) ranging from 58 nm (MMH, beech) to 128 nm (SS-18, birch) (Table S4). For pellets, peat, and diesel, the GMD values were 58, 64, and 44 nm, respectively.

The mean MCEs for wood log combustion varied from 0.94 to 0.98, with the lowest values observed in the SS experiments (Table S2). These values were notably higher than typical values reported for residential wood combustion in developing countries (Andreae, 2019) but were in the range of European and North American wood log stoves (Tasoglou et al., 2017; Price-Allison et al., 2021). An increase in the fuel moisture content decreased MCE values which is in agreement with the previous studies (Fig. S6b) (e.g., Price-Allison et al., 2021, 2019). For the pellet boiler, the MCE was 0.998 ± 0.002, indicating a nearly complete combustion. Generally, an MCE value less than 0.9 refers to smoldering combustion and higher values correspond to flaming combustion (Reid et al., 2005; Shen et al., 2011). Based on this, all the experiments could be classified as flaming combustion, although our experiments also include the ignition phase and residual char burning phases. There was no observed correlation between the MCE and EC or eBC emissions, but there was a slight negative correlation ($R^2 = 0.62$, $p = 0.001$) between average OC emissions and MCE for the fuel–appliance combinations (Fig. S7).

3.2 eBC absorption and $MAC_{880\,nm}$

The potential differences in the absorption efficiency of soot emitted from the different combustion sources were investigated by determining the mass absorption cross-section of BC ($MAC_{880\,nm}$) for each fuel–appliance combination based on the linear regression model between $b_{abs(880\,nm)}$ and EC mass concentrations. However, it is important to note that since we did not have a reference optical instrument to correct for potential bias in the aerosol multiple scattering coefficient (C) (Kumar et al., 2018; Tasoglou et al., 2017; Olson et al., 2015; Wu et al., 2021), the absolute $MAC_{880\,nm}$ values should be treated as indicative. Among the wood log combustion appliances, the $MAC_{880\,nm}$ ranged between $8.41 \pm 1.34\,\mathrm{m^2\,g^{-1}}$ (CMH, birch) and $15.0 \pm 5.49\,\mathrm{m^2\,g^{-1}}$ (MCS, beech) (Fig. 2b). Interestingly, the average $MAC_{880\,nm}$ for each wood species with similar moisture content did not differ significantly even when combusted in different appliances. However, the beech logs showed an exception with a $MAC_{880\,nm}$ of $9.98 \pm 4.13\,\mathrm{m^2\,g^{-1}}$ in MMH and $15.0 \pm 5.49\,\mathrm{m^2\,g^{-1}}$ in MCS. Overall, the average $MAC_{880\,nm}$ values for pine and spruce log combustion were 12.2 ± 2.02 and $13.3 \pm 2.05\,\mathrm{m^2\,g^{-1}}$, respectively, which were higher compared with birch ($9.40 \pm 1.65\,\mathrm{m^2\,g^{-1}}$). The

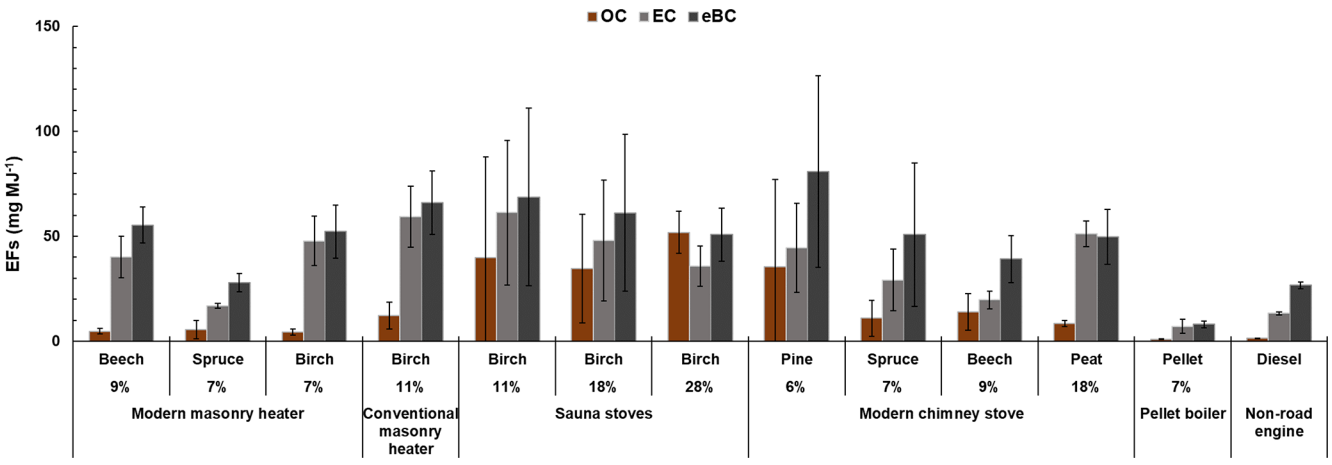

Figure 1. Average EFs (in mg $MJ^{-1} \pm$ standard deviation of the means) for organic carbon (OC), elemental carbon (EC), and equivalent black carbon (eBC) concentrations. The percentages indicate the fuel moisture content.

$MAC_{880\,nm}$ for pellet burning was $8.16 \pm 2.84\ m^2\ g^{-1}$ and for NrDE $15.6 \pm 0.75\ m^2\ g^{-1}$.

Higher $MAC_{880\,nm}$ values were found for the modern stoves compared with conventional and sauna stoves. This might be a consequence of different nanostructures and the maturity of soot between traditional and advanced appliances. A similar difference has been previously observed for simple and improved cook stoves (Wu et al., 2021; Saliba et al., 2018). We further hypothesized that $MAC_{880\,nm}$ values may be related to the particle number size distribution (Romshoo et al., 2021); however, no correlation was seen between GMD and $MAC_{880\,nm}$ (Fig. S8).

The $MAC_{880\,nm}$ increased with increasing fuel moisture content, as observed in the SS experiments (Figs. 2b and S9a). The OC / EC ratio showed a moderate correlation with $MAC_{880\,nm}$ (Fig. S10), suggesting that the increase in $MAC_{880\,nm}$ might be caused by the increased organic coating enhancing the lensing to the absorbing EC core (Bond et al., 2006; Jacobson, 2000, 2001). $MAC_{880\,nm}$ might also be enhanced by the presence of organic matter absorbing light at the higher wavelengths. Specifically, tar-ball-like morphologies in biomass combustion particles have been associated with a wide absorption wavelength range (Hoffer et al., 2016). In previous studies, tar-ball-like morphologies were not observed in the emissions of the wood-fired modern chimney stove (Leskinen et al., 2023) or the masonry heater (Leskinen et al., 2014). However, the less-efficient wood combustion conditions may promote the formation of tar-ball-like particles (Pósfai et al., 2004).

The direct comparison of MACs from different studies is often hindered by differences in instrumentation, as large differences between $MAC_{880\,nm}$ can be derived even for the same experiment using different BC measurement methods (Healy et al., 2017). Kumar et al. (2018) found beech log combustion soot to have a $MAC_{880\,nm}$ of $4.7\ m^2\ g^{-1}$ based on multi-wavelength absorption analyzer (MWAA) measurements, while Tasoglou et al. (2017) derived a $MAC_{532\,nm}$ of 8.56 and $8.98\ m^2\ g^{-1}$ for pine and birch bark, respectively, using a photoacoustic extinctiometer and refractory BC from the soot particle aerosol mass spectrometer in their measurements. The aethalometer, on the other hand, measures light attenuation, making our results sensitive to potential discrepancies in the filter multiple scattering. Here, we applied the C values given by the instrument manufacturer for the filter tapes used. Previous studies have, however, determined C values of 3 for wood log combustion (Kumar et al., 2018) and 2.29–3.45 for ambient air measurements (Yus-Díez et al., 2021; Backman et al., 2017). By using a C value of 3, the MAC factors determined in this work decreased by a factor of $\sim 50\,\%$ and correspond to the range of 4–$7\ m^2\ g^{-1}$ for wood log combustion (Fig. 2b) which is generally in agreement with values reported by Kumar et al. (2018) and Olson et al. (2015). Similarly, using a C value of 3, the $MAC_{880\,nm}$ of pellet burning ($4.27\ m^2\ g^{-1}$) was comparable to that of the previously studied natural draft pellet-fired stove with AE31 and a photoacoustic extinctiometer (Olson et al., 2015). However, even with the C value of 3, the $MAC_{880\,nm}$ of NrDE ($8.16\ m^2\ g^{-1}$) remains higher compared with that of previous studies (Olson et al., 2015; Wu et al., 2021). This difference in $MAC_{880\,nm}$ for diesel engine exhausts may be due to the differences in engine and exhaust after-treatment technologies. Our test engine was a small NrDE (single-person driven lawnmower) without any emission after-treatment technologies, while the previously reported MAC values are predominantly for heavy-duty vehicles equipped with exhaust after-treatment systems, such as diesel oxidation catalyst and exhaust gas recirculation. These after-treatment systems have been previously shown to alter soot nanostructure, which also likely influences the soot's optical properties (Malmborg et al., 2017).

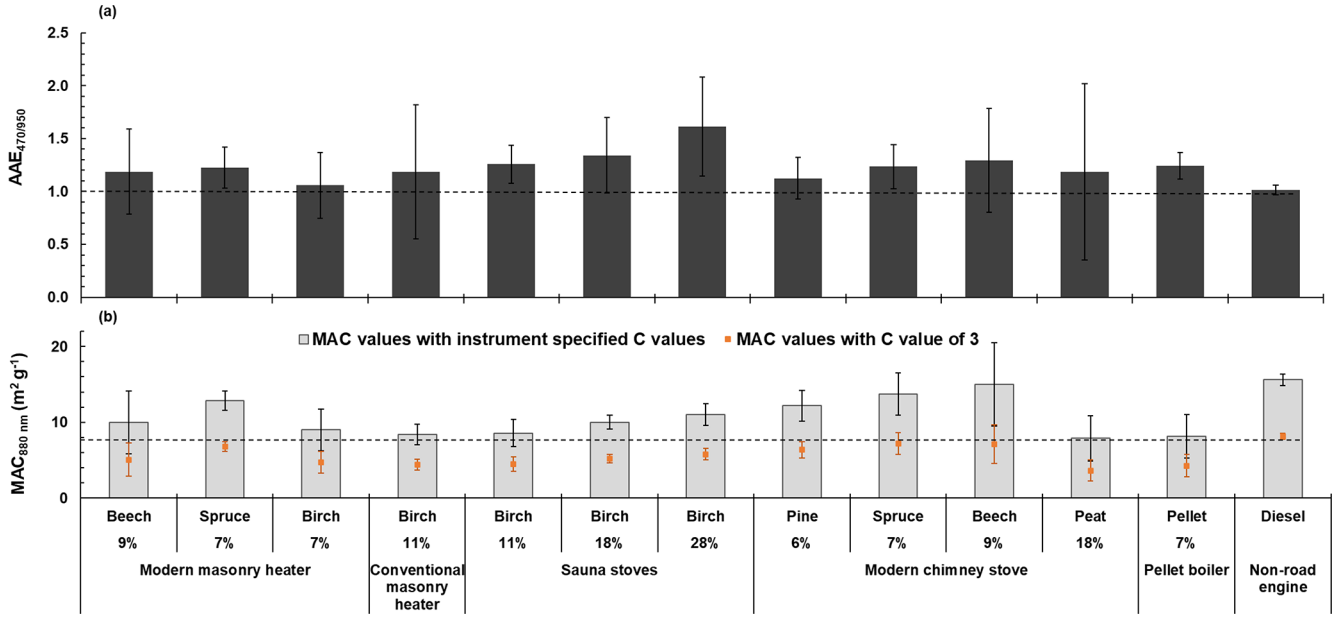

Figure 2. Optical properties of aerosols emitted from different combustion processes: average **(a)** $AAE_{470/950}$ and **(b)** $MAC_{880\,nm}$ from different emission sources, applying the default C values (gray bars) and with a C value of 3 (orange dots). The common threshold value of $AAE = 1$ for pure BC and the default MAC_{aeth} for 880 nm ($7.77\,m^2\,g^{-1}$) are shown as dashed lines for reference. Error bars illustrate the standard deviations of the means over whole burn cycles. The percentages indicate the fuel moisture content.

3.3 Absorption Ångström exponents

The two-wavelength AAE ($AAE_{470/950}$) model is used widely in the literature and is currently a standard method applied for the source apportionment of ambient aerosols. Thus, here we focus the discussion on $AAE_{470/950}$. Generally, the $AAE_{470/950}$ and $AAE_{370–950}$ were in line, with a slightly higher $AAE_{470/950}$ compared with the $AAE_{370–950}$. The average $AAE_{470/950}$ for full experiments using moderately dry (7 %–11 % moisture content) wood log combustion varied between 1.06 ± 0.31 (MMH, birch) and 1.26 ± 0.18 (SS-11, birch) (Fig. 2a). These values are similar to previously studied fresh emissions from wood combustion (Helin et al., 2021; Kumar et al., 2018; Grieshop et al., 2017; Tasoglou et al., 2017; Martinsson et al., 2015; Saleh et al., 2013) but notably lower than the assumption of $AAE = 2$, which is the standard used by the aethalometer ambient source apportionment for biomass burning (Sandradewi et al., 2008). The source apportionment method would, in other words, fail to account for the sources of fossil fuel and wood burning in this study. $AAE_{470/950}$ for the NrDE exhaust was 1.02 ± 0.05, which agrees with the general assumption of $AAE \sim 1$ for fossil fuel sources. Similar results for diesel engines have been obtained in previous studies irrespective of the engine types or after-treatment technologies used (Helin et al., 2021; Olson et al., 2015).

The design of the sauna stove had minimal influence on the $AAE_{470/950}$ when dry fuel was used, as shown in Fig. S9b. However, when the fuel moisture content increased from 11 % to 28 %, the $AAE_{470/950}$ changed from 1.26 ± 0.18 to 1.61 ± 0.47 (Fig. 2a; Table S5). This change in $AAE_{470/950}$ can be attributed to differences in the fuel moisture content affecting the combustion conditions in the stove, with higher $AAE_{470/950}$ associated with lower average MCEs (Fig. 3b). This suggests that more BrC was produced during less-efficient combustion conditions. A similar converse relationship has been also previously observed (Zhang et al., 2020; Pokhrel et al., 2016; Tian et al., 2019; Zhang et al., 2021).

The $AAE_{470/950}$ of wood combustion exhaust correlated with the OC / EC ratio ($R^2 = 0.79$, $p < 0.001$; Fig. 3a) due to the BrC constituents in the OC increasing the absorption specifically at the lower wavelengths. Consequently, $BrC_{370–950}$ showed a very good correlation with $AAE_{470/950}$, as expected ($R^2 = 0.87$, $p < 0.001$; Fig. S11). In addition to the presence of light-absorbing organic material in the particles, variation in the AAE indicates changes in the extent of lensing of different wavelengths, which is impacted by the morphology, BC core particle size, and coating thickness (Virkkula, 2021; He et al., 2015; Gyawali et al., 2009; Luo et al., 2023).

The temporal diversity in the $AAE_{470/950}$ is illustrated for all the different fuel and combustion appliance combinations used in this study in the exemplary time series of data in Fig. S12. High variability in wood combustion $AAE_{470/950}$ can be observed between the different combustion phases (Fig. S12a, b, e, g, and h). The addition of a new batch of wood logs onto the glowing embers led to rapid, low-temperature pyrolysis of volatile organics result-

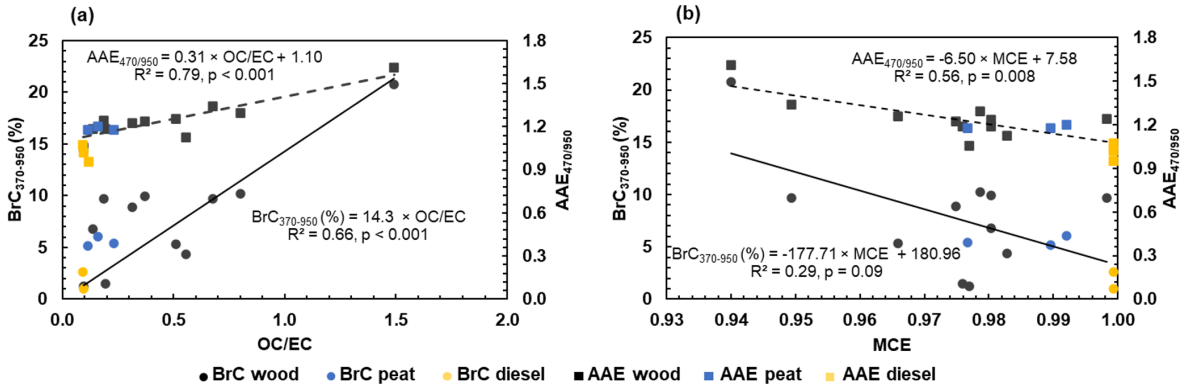

Figure 3. Relationships between **(a)** $AAE_{470/950}$ and $BrC_{370–950}$ (%) versus OC / EC and **(b)** dependence of $AAE_{470/950}$ and $BrC_{370–950}$ (%) on MCE for individual combustion fuel–appliance combinations. The slopes are calculated for wood combustion, i.e., data for peat and diesel were not considered.

ing in high organic aerosol (OA) emissions (Kortelainen et al., 2018). Consequently, the highest $AAE_{470/950}$ (1.5–2.5) was recorded during the ignition phase of each new batch (Fig. S12a, b, and e). As the flaming phase started, the combustion temperature increased with BC dominating over OA, resulting in a decrease of $AAE_{470/950}$ values to 1.0–1.5 (Fig. S12a, b, e, and g). Similar observations were reported by Martinsson et al. (2015), with AAEs of exhaust from traditional Scandinavian wood stoves ranging from 1.0 to 1.2 during flaming phase combustion and 2.5 to 2.7 during the ignition phase from batch-wise combustion.

Peat had a constant $AAE_{470/950}$ of 1.2–1.3 for the flaming phase with high variability in the ember phase as soon as fuels were consumed before the addition of the next batch (Fig. S12f). NrDE use and pellet combustion, on the other hand, had constant $AAE_{470/950}$ values throughout the whole experiment (Fig. S12c and d).

The validity of the general assumption of $AAE_{BC} = 1$ for pure BC particles cannot be directly confirmed with this instrumentation, but it can be reviewed by considering the particles with minimal organic matter content. For example, the particulate exhaust from the birch log combustion in the MMH had a carbonaceous fraction consisting of 91.7 % EC and yielded an $AAE_{470/950}$ of 1.06, relatively closely matching the general assumption of $AAE_{BC} = 1$. Similarly, diesel engine particles with an EC fraction of 90.8 % had an $AAE_{470/950}$ of 1.02. Furthermore, the validity of the assumption can be examined by extrapolating the correlation between $AAE_{470/950}$ and OC / EC (Fig. 3a). Based on the regression model, RWC soot consisting purely of EC (OC / EC = 0) would have an $AAE_{470/950}$ of 1.1.

In general, our study showed $AAE_{470/950}$ values below 1.4 in fresh exhaust from residential combustion of dry wood. However, ambient aerosols do not only include freshly emitted particles but are a mixture of primary and secondary aerosols. The mixing is both internal (i.e., different chemical compounds are assumed to be mixed in particles for a given particle size) and external (i.e., no physical or chemical interaction occurs between different particle compounds as different chemical compounds are assumed to be present in separate particles). As a result of atmospheric processing, aged emissions may have different $AAE_{470/950}$ values compared with those for freshly produced aerosols. This is due to possible BrC formation or loss from the oxidation and functionalization reactions of organic matter in the atmosphere (Yang et al., 2021; Liu-Kang et al., 2022; Hems and Abbatt, 2018), changes in the lensing by particle coating (Gyawali et al., 2009; Lack and Cappa, 2010; Hems et al., 2021), and other morphological changes in particle structure (Leskinen et al., 2023). Thus, lower $AAE_{470/950}$ values in this study compared with the ambient wood-burning aerosols may be partially explained as being due to the lack of atmospheric aging of measured emissions.

3.4 Absorption by BrC

The total absorption coefficients below the wavelength of 880 nm were higher than those extrapolated for BC at $AAE_{BC} = 1$, indicating the presence of BrC and potentially also the enhanced lensing effect due to the coating of soot particles. Figure 4 summarizes the total absorption coefficients by BrC for the different combustion appliances, with the absorption by BrC in MMH and MCS (Fig. 4a and c, respectively) given as the combinations of the different fuel types (beech, spruce, and birch for MMH, and pine, spruce, and beech for MCS). The average $BrC_{370–950}$ is given for all the individual fuel–appliance combinations in Fig. 5. For wood log combustion, $BrC_{370–950}$ ranged from 1.28 % for birch with 7 % moisture content up to 20.8 % for birch with 28 % moisture content (Fig. 5). Surprisingly, peat combustion displayed a relatively low $BrC_{370–950}$ (5.98 %) at 18 % moisture content (Fig. 5), presumably because of the prevalent flaming combustion resulting in minimal organic emissions. In the case of NrDE use, $BrC_{370–950}$ was negligible

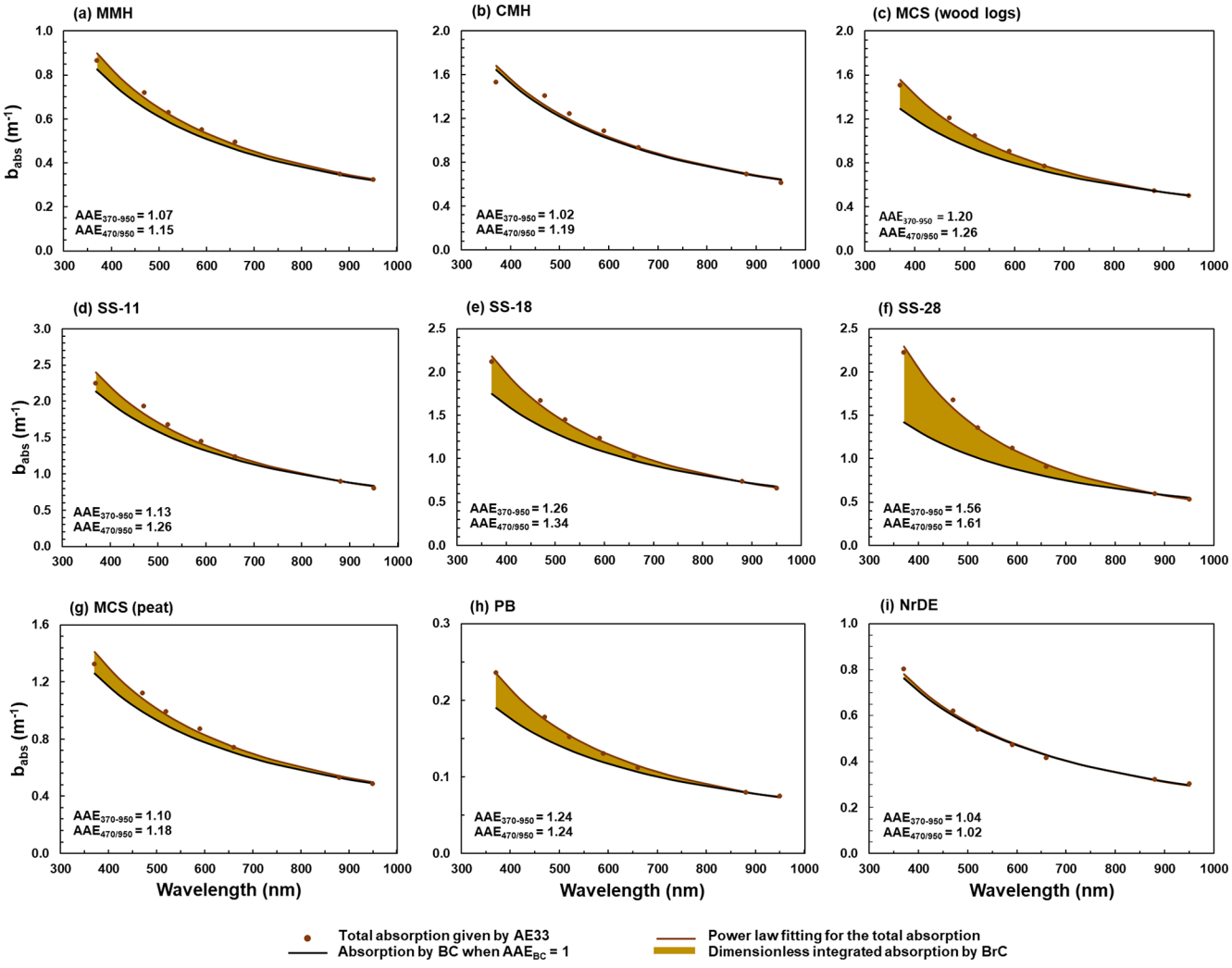

Figure 4. Absorption (per meter in the raw exhaust (plume) gas concentration) by $BrC_{370–950}$ summarized for combustion appliances: **(a)** MMH, **(b)** CMH, **(c)** MCS with wood logs, **(d)** SS-11 with 11 % fuel moisture content, **(e)** SS-18 with 18 % fuel moisture content, **(f)** SS-28 with 28 % fuel moisture content, **(g)** MCS with peat, **(h)** PB, and **(i)** NrDE. The brown markers indicate the total absorption given by AE33, while the brown line represents the power law fitting for the total absorption given by AE33. The black line represents the absorption by BC when $AAE_{BC} = 1$, and the difference between the total absorption and absorption by BC, shown by a light-brown area, indicates the dimensionless integrated absorption by BrC.

(0.66 %) (Fig. 5), consistent with expectations based on prior studies (Sandradewi et al., 2008). This marginal BrC absorption can be attributed to internal mixing, as diesel engines are not anticipated to generate aerosols containing BrC (Malmborg et al., 2021). The $BrC_{370–950}$ varied between different combustion events similarly to the $AAE_{470/950}$, as illustrated in Fig. S12.

The relative contribution of BrC to the absorption at 470 nm was higher than at other wavelengths for most of the experiments (Fig. 4; Table S6), resulting in lower $AAE_{370–950}$ compared with $AAE_{470/950}$. The average $BrC_{370–950}$ was approximately 60 % of the contribution of BrC exclusively at 470 nm (Fig. 6). Although BrC has a significant presence and absorption capability across a broader spectral range, the evaluation of BrC absorption often focuses on specific wavelengths, such as 370 or 470 nm. In a study conducted by Martinsson et al. (2015) with birch log combustion, BrC accounted for 20 %–75 % of the absorption at lower wavelengths during the ignition phase. The BrC absorption decreased with increasing wavelengths and was reported to account for 45 %–65 % at 520 nm. Similarly, Pokhrel et al. (2017) reported a wide range for the contribution of BrC to absorption at 405 nm (from 0 % to 92 %) and 532 nm (up to 58 %) for biomass combustion exhausts depending on the utilized segregation method, while Fang et al. (2022) observed BrC absorption ranging from 33 % to 90 % at 370 nm during different biomass burning experiments. The environmental significance of the absorptivity at

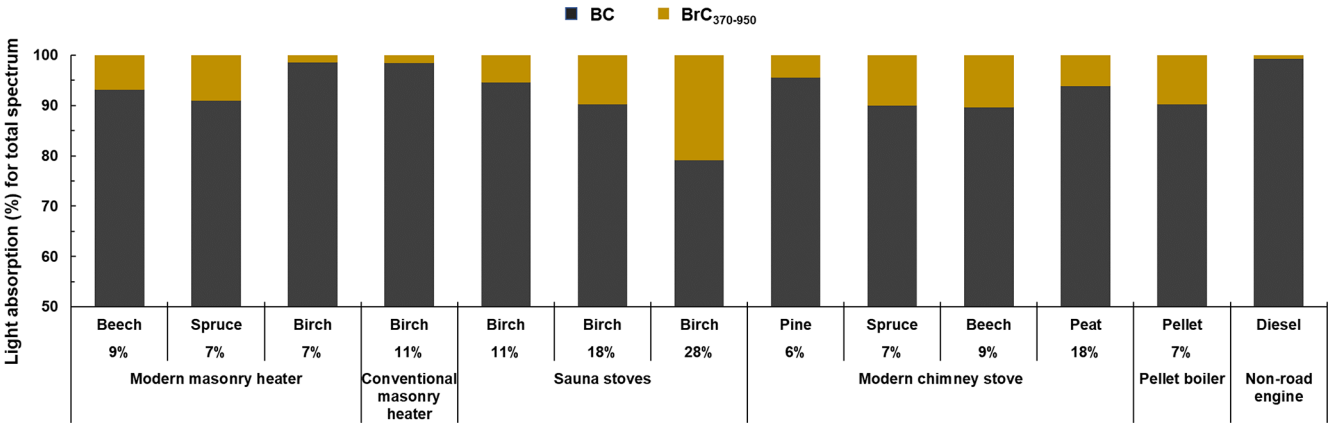

Figure 5. Contribution of BC and BrC to the total absorption over the wavelength range 370–950 nm for different fuel types and combustion appliances ($AAE_{BC} = 1$). The percentages indicate the fuel moisture content.

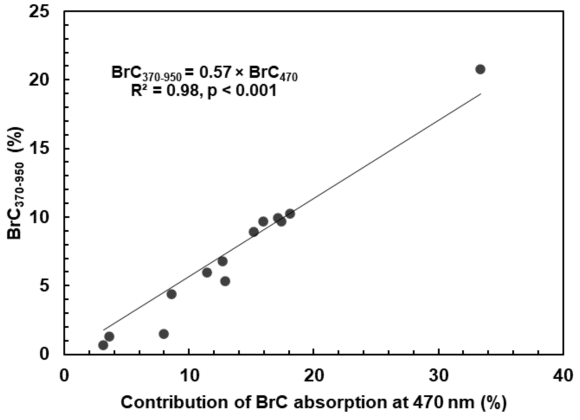

Figure 6. The average contributions of BrC to the absorption at 470 nm versus the total contribution over the wavelength range of 370–950 nm for all the fuel–appliance combinations.

different wavelengths also depends on the spectral abundance in the atmosphere. The relative contribution of BrC to the absorptivity in the visible wavelength range remains close to that of $BrC_{370–950}$ also if the absorptions illustrated in Fig. 4 are weighted by the standard solar irradiance spectra (ASTM G173-03; Fig. S13). However, to comprehensively describe the BrC impact on radiative forcing, future studies should include a description of the BrC contribution to the absorption across the visible wavelength range as well as the light scattering by the aerosol.

The contribution of BrC depends on the applied AAE_{BC} values, which are indicative of the spectral dependence of absorption by the BC. The sensitivity of the BrC contribution to the chosen AAE_{BC} value depends on the amount of BrC, as depicted in Figs. S14 and S15. The relative uncertainty associated with the assumed AAE_{BC} increases when the fraction of BrC in the emissions is low. For instance, assuming an AAE_{BC} of 0.9 led to an almost 4-fold increase (from 1.28 % to 5.07 %) in the contribution of BrC for dry birch wood and an almost 7-fold increase (from 0.66 % to 4.47 %) for diesel fuel when compared with the initial shares that had an AAE_{BC} of 1.0. In contrast, when an AAE_{BC} of 1.1 was assumed, the absorption was completely dominated by BC for these fuels.

The average $BrC_{370–950}$ of the studied fuel–appliance combinations had a good correlation with the OC / EC ratio ($R^2 = 0.66$; Fig. 3a). An increase of one unit in the OC / EC ratio corresponded to a 14 % increase in the $BrC_{370–950}$. The correlation of $BrC_{370–950}$ with the OC fraction (Fig. S16) suggests that the fraction of absorption by BrC can become a major contributor to UV and near-UV absorption if a significant amount of OC is present in the exhaust emission. Also, the MCE had a slight relationship with the BrC absorption, the overall trend showing that lower MCE values correspond to higher $BrC_{370–950}$, which is in agreement with previous findings concerning open biomass burning (Pokhrel et al., 2017; H. Li et al., 2019).

The $MAC_{OC,470\,nm}$ had high variability (24.1 ± 6.44 to $2.39 \pm 5.86\,m^2\,g^{-1}$) for the different fuel–appliance combinations, with no clear trend between the $MAC_{OC,470\,nm}$ and the amount of OC. This variation may be due to differences in the chemical composition of the organic fraction or the extent of the lensing effect with varying coating amounts, and determination of the exact MAC_{OC}s would require further investigation of the pure organic fraction from different combustion conditions.

4 Conclusions

In this study, we characterized the emissions of BrC originating from various wood combustion appliances in northern Europe based on the wavelength-dependent aerosol absorption data from a seven-wavelength aethalometer and thermal–optical carbon analysis of particle filter samples. By utilizing the information from all seven wavelengths of the

aethalometer, we derived an integrated parameter to account for the total BrC absorption across the visible light spectrum. The $BrC_{370–950}$ varied greatly (ranging from 1.28 % to 20.8 %) for wood log combustion events and was primarily influenced by fuel moisture content and modified combustion efficiency but also by the combustion appliance type. The highest $BrC_{370–950}$ contributions were observed for the fuels with the highest moisture contents due to the decreased combustion efficiency. Furthermore, correlations between the OC / EC ratios and $BrC_{370–950}$ demonstrated that a one-unit increase in OC / EC would correspond to an approximately 14 % increase in $BrC_{370–950}$. These findings confirm that BrC can be a significant contributor to UV and near-UV light absorption in wood stove emissions from northern Europe, when OC / EC ratios are high, and may offer a useful parameterization for assessing the BrC emissions from different RWC designs.

The study also reviewed the commonly used assumption of an AAE of 2 for source apportionment of wood-burning emissions. The $AAE_{470/950}$ values obtained in this study ranged from 1.06 to 1.61 for wood log combustion, suggesting that the assumed value of AAE = 2 might be too high for northern European RWC emissions. However, it should be noted that the presented $AAE_{470/950}$ values were determined for fresh aerosols, and atmospheric transformation is likely to influence these values. By extrapolating the correlation between $AAE_{470/950}$ and OC / EC, it was found that pure RWC black carbon particles would exhibit an $AAE_{470/950}$ close to unity, which aligns with the general assumption used to differentiate the light absorption caused by black carbon and brown carbon. Additionally, exhaust from a non-road diesel engine was found to have an $AAE_{470/950}$ of 1.02, matching well the assumptions used in source apportionment. During the wood log combustion process, both the $BrC_{370–950}$ contribution and $AAE_{470/950}$ varied substantially, with the ignition phase exhibiting higher BrC contributions compared with the flaming phase. This disparity can be attributed to the introduction of a new batch of wood logs onto the glowing embers, resulting in rapid, low-temperature pyrolysis of volatile organics and subsequent high emissions of organic aerosols.

Overall, this study provides valuable data for the estimation of BrC emissions from northern European RWC. In addition to providing BC emission factors for modern RWC appliances, these findings can aid in integrating the BrC-induced absorption in emission inventory assessments using the multi-wavelength aethalometer data from air quality monitoring networks. However, further research concerning different combustion conditions and fuel qualities of RWC, especially high moisture content fuels, and low combustion efficiencies, is needed to comprehensively evaluate the role of BrC in particle light absorption for RWC in other regions.

Appendix A: List of abbreviations

$AAE_{470/950}$	absorption Ångström exponent for the wavelength pair 470 and 950 nm
$AAE_{370–950}$	absorption Ångström exponent attained by fitting power law to the total absorption given by AE33
AAE_{BC}	absorption Ångström exponent for pure black carbon
AE33	aethalometer model 33
b_{abs}	absorption coefficient
BB	biomass burning
BC	black carbon
BrC	brown carbon
$BrC_{370–950}$	contribution of BrC to the total absorption over wavelengths 370–950 nm
CMH	conventional masonry heater
DR	dilution ratio
eBC	equivalent black carbon
EC	elemental carbon
ED	ejector diluter
EF	emission factor
GMD	number-based geometric mean diameter
ILMARI	Aerosol physics, chemistry, and toxicology research unit
IMPROVE	Interagency Monitoring of Protected Visual Environments
MAC	mass absorption cross-section
MAC_{aeth}	standard mass absorption cross-section applied by AE33
$MAC_{880\,nm}$	measured mass absorption cross-section of BC (880 nm)
MAC_{OC}	measured mass absorption cross-section of the organic fraction
MCE	modified combustion efficiency
MCS	modern chimney stove
MMH	modern masonry heater
NIOSH	National Institute for Occupational Safety and Health
NrDE	non-road diesel engine
OA	organic aerosol
OC	organic carbon
PB	pellet boiler
PM	particulate matter
RWC	residential wood combustion
SIMO	residential wood combustion simulator
SS	sauna stoves
SD	standard deviation
UV	ultraviolet

Data availability. Further experimental data will be provided upon request to the corresponding authors.

Supplement. The supplement contains additional information on the experimental conditions, a description of BrC uncertainty calculation, and other experimental results to support the findings of this study. The supplement related to this article is available online at: https://doi.org/10.5194/acp-24-3197-2024-supplement.

Author contributions. OS, AK, RZ, and JT supervised and acquired funding for the study. MI, PYP, OS, GJ, MK, HS, SV, JL, MS, JT, SB, LK, and AH designed and performed the experiments. SB, AH, OS, SV, MK, AV, and HS analyzed and evaluated the data. SB, AH, and OS wrote the paper with input and approval from all authors.

Competing interests. The contact author has declared that none of the authors has any competing interests.

Disclaimer. Publisher's note: Copernicus Publications remains neutral with regard to jurisdictional claims made in the text, published maps, institutional affiliations, or any other geographical representation in this paper. While Copernicus Publications makes ev-

ery effort to include appropriate place names, the final responsibility lies with the authors.

Acknowledgements. This work was supported by the Finnish Cultural Foundation, North Karelia, and North Savo Funds (AERO-LCA project, grant nos. 55201441 and 65202068), the Research Council of Finland (BBrCAC project, grant no. 341597), the "KIUAS-2" project, and the Helmholtz Virtual Institute of Complex Molecular Systems in Environmental Health, Aerosols and Health (HICE) funded by the Initiative and Networking Fund of the Helmholtz Association (HGF, Germany). ChatGPT-3, an Open AI tool, was consulted for paraphrasing the "Conclusions" section of the paper.

Financial support. This research has been supported by the Finnish Cultural Foundation North Karelia and North Savo Funds (grant nos. 55201441 and 65202068), Research Council of Finland (grant no. 341597), the KIUAS-2 project, and the Helmholtz Virtual Institute of Complex Molecular Systems in Environmental Health, Aerosols and Health (HICE) funded by the Initiative and Networking Fund of the Helmholtz Association (HGF, Germany).

Review statement. This paper was edited by Alexander Laskin and reviewed by two anonymous referees.

References

Andreae, M. O.: Emission of trace gases and aerosols from biomass burning – an updated assessment, Atmos. Chem. Phys., 19, 8523–8546, https://doi.org/10.5194/acp-19-8523-2019, 2019.

Backman, J., Schmeisser, L., Virkkula, A., Ogren, J. A., Asmi, E., Starkweather, S., Sharma, S., Eleftheriadis, K., Uttal, T., Jefferson, A., Bergin, M., Makshtas, A., Tunved, P., and Fiebig, M.: On Aethalometer measurement uncertainties and an instrument correction factor for the Arctic, Atmos. Meas. Tech., 10, 5039–5062, https://doi.org/10.5194/amt-10-5039-2017, 2017.

Bahadur, R., Praveen, P. S., Xu, Y., and Ramanathan, V.: Solar absorption by elemental and brown carbon determined from spectral observations, P. Natl. Acad. Sci. USA, 109, 17366–17371, https://doi.org/10.1073/pnas.1205910109, 2012.

Bernardoni, V., Pileci, R. E., Caponi, L., and Massabò, D.: The multi-wavelength absorption analyzer (MWAA) model as a tool for source and component apportionment based on aerosol absorption properties: Application to samples collected in different environments, Atmosphere, 8, 218, https://doi.org/10.3390/atmos8110218, 2017.

Bond, T. C., Habib, G., and Bergstrom, R. W.: Limitations in the enhancement of visible light absorption due to mixing state, J. Geophys. Res.-Atmos., 111, 20211, https://doi.org/10.1029/2006JD007315, 2006.

Bond, T. C., Doherty, S. J., Fahey, D. W., Forster, P. M., Berntsen, T., Deangelo, B. J., Flanner, M. G., Ghan, S., Kärcher, B., Koch, D., Kinne, S., Kondo, Y., Quinn, P. K., Sarofim, M. C., Schultz, M. G., Schulz, M., Venkataraman, C., Zhang, H., Zhang, S., Bellouin, N., Guttikunda, S. K., Hopke, P. K., Jacobson, M. Z., Kaiser, J. W., Klimont, Z., Lohmann, U., Schwarz, J. P., Shindell, D., Storelvmo, T., Warren, S. G., and Zender, C. S.: Bounding the role of black carbon in the climate system: A scientific assessment, J. Geophys. Res.-Atmos., 118, 5380–5552, https://doi.org/10.1002/jgrd.50171, 2013.

Briggs, N. L. and Long, C. M.: Critical review of black carbon and elemental carbon source apportionment in Europe and the United States, Atmos. Environ., 144, 409–427, https://doi.org/10.1016/j.atmosenv.2016.09.002, 2016.

Cappa, C. D., Zhang, X., Russell, L. M., Collier, S., Lee, A. K. Y., Chen, C. L., Betha, R., Chen, S., Liu, J., Price, D. J., Sanchez, K. J., McMeeking, G. R., Williams, L. R., Onasch, T. B., Worsnop, D. R., Abbatt, J., and Zhang, Q.: Light Absorption by Ambient Black and Brown Carbon and its Dependence on Black Carbon Coating State for Two California, USA, Cities in Winter and Summer, J. Geophys. Res.-Atmos., 124, 1550–1577, https://doi.org/10.1029/2018JD029501, 2019.

Cheng, Y., He, K.-B., Zheng, M., Duan, F.-K., Du, Z.-Y., Ma, Y.-L., Tan, J.-H., Yang, F.-M., Liu, J.-M., Zhang, X.-L., Weber, R. J., Bergin, M. H., and Russell, A. G.: Mass absorption efficiency of elemental carbon and water-soluble organic carbon in Beijing, China, Atmos. Chem. Phys., 11, 11497–11510, https://doi.org/10.5194/acp-11-11497-2011, 2011.

Chow, J. C., Watson, J. G., Chen, L.-W. A., Chang, M. C. O., Robinson, N. F., Trimble, D., and Kohl, S.: The IMPROVE_A Temperature Protocol for Thermal/Optical Carbon Analysis: Maintaining Consistency with a Long-Term Database, J. Air Waste Manage. Assoc., 57, 1014–1023, https://doi.org/10.3155/1047-3289.57.9.1014, 2007.

Czech, H., Miersch, T., Orasche, J., Abbaszade, G., Sippula, O., Tissari, J., Michalke, B., Schnelle-Kreis, J., Streibel, T., Jokiniemi, J., and Zimmermann, R.: Chemical composition and speciation of particulate organic matter from modern residential small-scale wood combustion appliances, Sci. Total Environ., 612, 636–648, https://doi.org/10.1016/J.SCITOTENV.2017.08.263, 2018.

Drinovec, L., Močnik, G., Zotter, P., Prévôt, A. S. H., Ruckstuhl, C., Coz, E., Rupakheti, M., Sciare, J., Müller, T., Wiedensohler, A., and Hansen, A. D. A.: The "dual-spot" Aethalometer: an improved measurement of aerosol black carbon with real-time loading compensation, Atmos. Meas. Tech., 8, 1965–1979, https://doi.org/10.5194/amt-8-1965-2015, 2015.

Drinovec, L., Gregorič, A., Zotter, P., Wolf, R., Bruns, E. A., Prévôt, A. S. H., Petit, J.-E., Favez, O., Sciare, J., Arnold, I. J., Chakrabarty, R. K., Moosmüller, H., Filep, A., and Močnik, G.: The filter-loading effect by ambient aerosols in filter absorption photometers depends on the coating of the sampled particles, Atmos. Meas. Tech., 10, 1043–1059, https://doi.org/10.5194/amt-10-1043-2017, 2017.

EEA: European Union emission inventory report 1990–2014 under the UNECE Convention on Long-range Transboundary Air Pollution (LRTAP), EEA Technical report No. 10/2013, 1–142, https://doi.org/10.2800/44480, 2013.

Fang, Z., Deng, W., Wang, X., He, Q., Zhang, Y., Hu, W., Song, W., Zhu, M., Lowther, S., Wang, Z., Fu, X., Hu, Q., Bi, X., George, C., and Rudich, Y.: Evolution of light absorption properties during photochemical aging of straw open burning aerosols, Sci. Total Environ., 838, 156431, https://doi.org/10.1016/j.scitotenv.2022.156431, 2022.

Feng, Y., Ramanathan, V., and Kotamarthi, V. R.: Brown carbon: a significant atmospheric absorber of solar radiation?, Atmos. Chem. Phys., 13, 8607–8621, https://doi.org/10.5194/acp-13-8607-2013, 2013.

Grieshop, A. P., Jain, G., Sethuraman, K., and Marshall, J. D.: Emission factors of health- and climate-relevant pollutants measured in home during a carbon-finance-approved cookstove intervention in rural India, GeoHealth, 1, 222–236, https://doi.org/10.1002/2017GH000066, 2017.

Gyawali, M., Arnott, W. P., Lewis, K., and Moosmüller, H.: In situ aerosol optics in Reno, NV, USA during and after the summer 2008 California wildfires and the influence of absorbing and non-absorbing organic coatings on spectral light absorption, Atmos. Chem. Phys., 9, 8007–8015, https://doi.org/10.5194/acp-9-8007-2009, 2009.

Hartikainen, A., Tiitta, P., Ihalainen, M., Yli-Pirilä, P., Orasche, J., Czech, H., Kortelainen, M., Lamberg, H., Suhonen, H., Koponen, H., Hao, L., Zimmermann, R., Jokiniemi, J., Tissari, J., and Sippula, O.: Photochemical transformation of residential wood combustion emissions: dependence of organic aerosol composition on OH exposure, Atmos. Chem. Phys., 20, 6357–6378, https://doi.org/10.5194/acp-20-6357-2020, 2020.

He, C., Liou, K.-N., Takano, Y., Zhang, R., Levy Zamora, M., Yang, P., Li, Q., and Leung, L. R.: Variation of the radiative properties during black carbon aging: theoretical and experimental intercomparison, Atmos. Chem. Phys., 15, 11967–11980, https://doi.org/10.5194/acp-15-11967-2015, 2015.

Healy, R. M., Sofowote, U., Su, Y., Debosz, J., Noble, M., Jeong, C. H., Wang, J. M., Hilker, N., Evans, G. J., Doerksen, G., Jones, K., and Munoz, A.: Ambient measurements and source apportionment of fossil fuel and biomass burning black carbon in Ontario, Atmos. Environ., 161, 34–47, https://doi.org/10.1016/j.atmosenv.2017.04.034, 2017.

Helin, A., Virkkula, A., Backman, J., Pirjola, L., Sippula, O., Aakko-Saksa, P., Väätäinen, S., Mylläri, F., Järvinen, A., Bloss, M., Aurela, M., Jakobi, G., Karjalainen, P., Zimmermann, R., Jokiniemi, J., Saarikoski, S., Tissari, J., Rönkkö, T., Niemi, J. V., and Timonen, H.: Variation of Absorption Ångström Exponent in Aerosols From Different Emission Sources, J. Geophys. Res.-Atmos., 126, e2020JD034094, https://doi.org/10.1029/2020JD034094, 2021.

Hems, R. F. and Abbatt, J. P. D.: Aqueous Phase Photo-oxidation of Brown Carbon Nitrophenols: Reaction Kinetics, Mechanism, and Evolution of Light Absorption, ACS Earth Sp. Chem., 2, 225–234, https://doi.org/10.1021/acsearthspacechem.7b00123, 2018.

Hems, R. F., Schnitzler, E. G., Liu-Kang, C., Cappa, C. D., and Abbatt, J. P. D.: Aging of Atmospheric Brown Carbon Aerosol, ACS Earth Sp. Chem., 5, 722–748, https://doi.org/10.1021/acsearthspacechem.0c00346, 2021.

Hoffer, A., Tóth, A., Nyirő-Kósa, I., Pósfai, M., and Gelencsér, A.: Light absorption properties of laboratory-generated tar ball particles, Atmos. Chem. Phys., 16, 239–246, https://doi.org/10.5194/acp-16-239-2016, 2016.

Ihantola, T., Di Bucchianico, S., Happo, M., Happo, M., Ihalainen, M., Uski, O., Bauer, S., Kuuspalo, K., Kuuspalo, K., Sippula, O., Tissari, J., Oeder, S., Hartikainen, A., Rönkkö, T. J., Martikainen, M. V., Huttunen, K., Vartiainen, P., Suhonen, H., Kortelainen, M., Lamberg, H., Leskinen, A., Leskinen, A., Sklorz, M., Sklorz, M., Michalke, B., Dilger, M., Weiss, C., Dittmar, G., Beckers, J., Beckers, J., Beckers, J., Irmler, M., Buters, J., Candeias, J., Czech, H., Czech, H., Yli-Pirilä, P., Abbaszade, G., Jakobi, G., Orasche, J., Schnelle-Kreis, J., Kanashova, T., Kanashova, T., Karg, E., Streibel, T., Streibel, T., Passig, J., Hakkarainen, H., Jokiniemi, J., Zimmermann, R., Zimmermann, R., Hirvonen, M. R., and Jalava, P. I.: Influence of wood species on toxicity of log-wood stove combustion aerosols: A parallel animal and air-liquid interface cell exposure study on spruce and pine smoke, Part. Fibre Toxicol., 17, 1–26, https://doi.org/10.1186/s12989-020-00355-1, 2020.

IPCC: Climate Change 2014: Synthesis Report. Contribution of Working Groups I, II and III to the Fifth Assessment Report of the Intergovernmental Panel on Climate Change, edited by: Core Writing Team, Pachauri, R. K., and Meyer, L. A., IPCC, Geneva, Switzerland, 151 pp., ISBN 9789291691432, 2014.

Jacobson, M. Z.: A physically-based treatment of elemental carbon optics: Implications for global direct forcing of aerosols, Geophys. Res. Lett., 27, 217–220, https://doi.org/10.1029/1999GL010968, 2000.

Jacobson, M. Z.: Strong radiative heating due to the mixing state of black carbon in atmospheric aerosols, Nature, 409, 695–697, https://doi.org/10.1038/35055518, 2001.

Kirchstetter, T. W., Novakov, T., and Hobbs, P. V.: Evidence that the spectral dependence of light absorption by aerosols is affected by organic carbon, J. Geophys. Res.-Atmos., 109, 21208, https://doi.org/10.1029/2004JD004999, 2004.

Klimont, Z., Kupiainen, K., Heyes, C., Purohit, P., Cofala, J., Rafaj, P., Borken-Kleefeld, J., and Schöpp, W.: Global anthropogenic emissions of particulate matter including black carbon, Atmos. Chem. Phys., 17, 8681–8723, https://doi.org/10.5194/acp-17-8681-2017, 2017.

Kortelainen, M., Jokiniemi, J., Tiitta, P., Tissari, J., Lamberg, H., Leskinen, J., Grigonyte-Lopez Rodriguez, J., Koponen, H., Antikainen, S., Nuutinen, I., Zimmermann, R., and Sippula, O.: Time-resolved chemical composition of small-scale batch combustion emissions from various wood species, Fuel, 233, 224–236, https://doi.org/10.1016/j.fuel.2018.06.056, 2018.

Kumar, N. K., Corbin, J. C., Bruns, E. A., Massabó, D., Slowik, J. G., Drinovec, L., Močnik, G., Prati, P., Vlachou, A., Baltensperger, U., Gysel, M., El-Haddad, I., and Prévôt, A. S. H.: Production of particulate brown carbon during atmospheric aging of residential wood-burning emissions, Atmos. Chem. Phys., 18, 17843–17861, https://doi.org/10.5194/acp-18-17843-2018, 2018.

Lack, D. A. and Cappa, C. D.: Impact of brown and clear carbon on light absorption enhancement, single scatter albedo and absorption wavelength dependence of black carbon, Atmos. Chem. Phys., 10, 4207–4220, https://doi.org/10.5194/acp-10-4207-2010, 2010.

Lack, D. A. and Langridge, J. M.: On the attribution of black and brown carbon light absorption using the Ångström exponent, Atmos. Chem. Phys., 13, 10535–10543, https://doi.org/10.5194/acp-13-10535-2013, 2013.

Lack, D. A., Langridge, J. M., Bahreini, R., Cappa, C. D., Middlebrook, A. M., and Schwarz, J. P.: Brown carbon and internal mixing in biomass burning particles, P. Natl. Acad. Sci. USA, 109, 14802–14807, https://doi.org/10.1073/pnas.1206575109, 2012.

Lamberg, H., Sippula, O., Tissari, J., and Jokiniemi, J.: Effects of air staging and load on fine-particle and gaseous emissions from a small-scale pellet boiler, Energ. Fuel., 25, 4952–4960, https://doi.org/10.1021/ef2010578, 2011a.

Lamberg, H., Nuutinen, K., Tissari, J., Ruusunen, J., Yli-Pirilä, P., Sippula, O., Tapanainen, M., Jalava, P., Makkonen, U., Teinilä, K., Saarnio, K., Hillamo, R., Hirvonen, M. R., and Jokiniemi, J.: Physicochemical characterization of fine particles from small-scale wood combustion, Atmos. Environ., 45, 7635–7643, https://doi.org/10.1016/j.atmosenv.2011.02.072, 2011b.

Laskin, A., Laskin, J., and Nizkorodov, S. A.: Chemistry of Atmospheric Brown Carbon, Chem. Rev., 115, 4335–4382, https://doi.org/10.1021/cr5006167, 2015.

Leskinen, J., Ihalainen, M., Torvela, T., Kortelainen, M., Lamberg, H., Tiitta, P., Jakobi, G., Grigonyte, J., Joutsensaari, J., Sippula, O., Tissari, J., Virtanen, A., Zimmermann, R., and Jokiniemi, J.: Effective density and morphology of particles emitted from small-scale combustion of various wood fuels, Environ. Sci. Technol., 48, 13298–13306, https://doi.org/10.1021/es502214a, 2014.

Leskinen, J., Hartikainen, A., Väätäinen, S., Ihalainen, M., Virkkula, A., Mesceriakovas, A., Tiitta, P., Miettinen, M., Lamberg, H., Czech, H., Yli-Pirilä, P., Tissari, J., Jakobi, G., Zimmermann, R., and Sippula, O.: Photochemical Aging Induces Changes in the Effective Densities, Morphologies, and Optical Properties of Combustion Aerosol Particles, Environ. Sci. Technol., 57, 5137–5148, https://doi.org/10.1021/acs.est.2c04151, 2023.

Li, A. F., Zhang, K. M., Allen, G., Zhang, S., Yang, B., Gu, J., Hashad, K., Sward, J., Felton, D., and Rattigan, O.: Ambient sampling of real-world residential wood combustion plumes, J. Air Waste Manag. Assoc., 72, 710–719, https://doi.org/10.1080/10962247.2022.2044410, 2022.

Li, H., Lamb, K. D., Schwarz, J. P., Selimovic, V., Yokelson, R. J., McMeeking, G. R., and May, A. A.: Inter-comparison of black carbon measurement methods for simulated open biomass burning emissions, Atmos. Environ., 206, 156–169, https://doi.org/10.1016/j.atmosenv.2019.03.010, 2019.

Li, Z., Tan, H., Zheng, J., Liu, L., Qin, Y., Wang, N., Li, F., Li, Y., Cai, M., Ma, Y., and Chan, C. K.: Light absorption properties and potential sources of particulate brown carbon in the Pearl River Delta region of China, Atmos. Chem. Phys., 19, 11669–11685, https://doi.org/10.5194/acp-19-11669-2019, 2019.

Liu, C., Chung, C. E., Yin, Y., and Schnaiter, M.: The absorption Ångström exponent of black carbon: from numerical aspects, Atmos. Chem. Phys., 18, 6259–6273, https://doi.org/10.5194/acp-18-6259-2018, 2018.

Liu, J., Scheuer, E., Dibb, J., Diskin, G. S., Ziemba, L. D., Thornhill, K. L., Anderson, B. E., Wisthaler, A., Mikoviny, T., Devi, J. J., Bergin, M., Perring, A. E., Markovic, M. Z., Schwarz, J. P., Campuzano-Jost, P., Day, D. A., Jimenez, J. L., and Weber, R. J.: Brown carbon aerosol in the North American continental troposphere: sources, abundance, and radiative forcing, Atmos. Chem. Phys., 15, 7841–7858, https://doi.org/10.5194/acp-15-7841-2015, 2015.

Liu-Kang, C., Gallimore, P. J., Liu, T., and Abbatt, J. P. D.: Photoreaction of biomass burning brown carbon aerosol particles, Environ. Sci. Atmos., 2, 270–278, https://doi.org/10.1039/d1ea00088h, 2022.

Luo, J., Li, Z., Qiu, J., Zhang, Y., Fan, C., Li, L., Wu, H., Zhou, P., Li, K., and Zhang, Q.: The Simulated Source Apportionment of Light Absorbing Aerosols: Effects of Microphysical Properties of Partially-Coated Black Carbon, J. Geophys. Res.-Atmos., 128, e2022JD037291, https://doi.org/10.1029/2022JD037291, 2023.

Magnone, E., Park, S. K., and Park, J. H.: Effects of Moisture Contents in the Common Oak on Carbonaceous Aerosols Generated from Combustion Processes in an Indoor Wood Stove, Combust. Sci. Technol., 188, 982–996, https://doi.org/10.1080/00102202.2015.1136300, 2016.

Malmborg, V., Eriksson, A., Gren, L., Török, S., Shamun, S., Novakovic, M., Zhang, Y., Kook, S., Tunér, M., Bengtsson, P. E., and Pagels, J.: Characteristics of BrC and BC emissions from controlled diffusion flame and diesel engine combustion, Aerosol Sci. Tech., 55, 769–784, https://doi.org/10.1080/02786826.2021.1896674, 2021.

Malmborg, V. B., Eriksson, A. C., Shen, M., Nilsson, P., Gallo, Y., Waldheim, B., Martinsson, J., Andersson, Ö, and Pagels, J.: Evolution of In-Cylinder Diesel Engine Soot and Emission Characteristics Investigated with Online Aerosol Mass Spectrometry, Environ. Sci. Technol., 51, 1876–1885, https://doi.org/10.1021/acs.est.6b03391, 2017.

Martinsson, J., Eriksson, A. C., Nielsen, I. E., Malmborg, V. B., Ahlberg, E., Andersen, C., Lindgren, R., Nyström, R., Nordin, E. Z., Brune, W. H., Svenningsson, B., Swietlicki, E., Boman, C., and Pagels, J. H.: Impacts of Combustion Conditions and Photochemical Processing on the Light Absorption of Biomass Combustion Aerosol, Environ. Sci. Technol., 49, 14663–14671, https://doi.org/10.1021/acs.est.5b03205, 2015.

Massabò, D., Caponi, L., Bernardoni, V., Bove, M. C., Brotto, P., Calzolai, G., Cassola, F., Chiari, M., Fedi, M. E., Fermo, P., Giannoni, M., Lucarelli, F., Nava, S., Piazzalunga, A., Valli, G., Vecchi, R., and Prati, P.: Multi-wavelength optical determination of black and brown carbon in atmospheric aerosols, Atmos. Environ., 108, 1–12, https://doi.org/10.1016/J.ATMOSENV.2015.02.058, 2015.

NIOSH: Elemental Carbon (Diesel Particulate) Method 5040, in: NIOSH Manual of Analytical Methods (NMAM), The National Institute for Occupational Safety and Health, Atlanta, GA, https://doi.org/10.26616/NIOSHPUB2003154, 1999.

Olson, M. R., Garcia, M. V., Robinson, M. A., Van Rooy, P., Dietenberger, M. A., Bergin, M., and Schauer, J. J.: Investigation of black and brown carbon multiple-wavelength dependent light absorption from biomass and fossil fuel combustion source emissions, J. Geophys. Res., 120, 6682–6697, https://doi.org/10.1002/2014JD022970, 2015.

Olsen, Y., Nøjgaard, J. K., Olesen, H. R., Brandt, J., Sigsgaard, T., Pryor, S. C., Ancelet, T., Viana, M. del M., Querol, X., and Hertel, O.: Emissions and source allocation of carbonaceous air pollutants from wood stoves in developed countries: A review, Atmos. Pollut. Res., 11, 234–251, https://doi.org/10.1016/j.apr.2019.10.007, 2020.

Pani, S. K., Lin, N. H., Griffith, S. M., Chantara, S., Lee, C. Te, Thepnuan, D., and Tsai, Y. I.: Brown carbon light absorption over an urban environment in northern peninsular Southeast Asia, Environ. Pollut., 276, 116735, https://doi.org/10.1016/j.envpol.2021.116735, 2021.

Petzold, A., Ogren, J. A., Fiebig, M., Laj, P., Li, S.-M., Baltensperger, U., Holzer-Popp, T., Kinne, S., Pappalardo, G., Sug-

imoto, N., Wehrli, C., Wiedensohler, A., and Zhang, X.-Y.: Recommendations for reporting "black carbon" measurements, Atmos. Chem. Phys., 13, 8365–8379, https://doi.org/10.5194/acp-13-8365-2013, 2013.

Pokhrel, R. P., Wagner, N. L., Langridge, J. M., Lack, D. A., Jayarathne, T., Stone, E. A., Stockwell, C. E., Yokelson, R. J., and Murphy, S. M.: Parameterization of single-scattering albedo (SSA) and absorption Ångström exponent (AAE) with EC / OC for aerosol emissions from biomass burning, Atmos. Chem. Phys., 16, 9549–9561, https://doi.org/10.5194/acp-16-9549-2016, 2016.

Pokhrel, R. P., Beamesderfer, E. R., Wagner, N. L., Langridge, J. M., Lack, D. A., Jayarathne, T., Stone, E. A., Stockwell, C. E., Yokelson, R. J., and Murphy, S. M.: Relative importance of black carbon, brown carbon, and absorption enhancement from clear coatings in biomass burning emissions, Atmos. Chem. Phys., 17, 5063–5078, https://doi.org/10.5194/acp-17-5063-2017, 2017.

Pósfai, M., Gelencsér, A., Simonics, R., Arató, K., Li, J., Hobbs, P. V., and Buseck, P. R.: Atmospheric tar balls: Particles from biomass and biofuel burning, J. Geophys. Res.-Atmos., 109, D06213, https://doi.org/10.1029/2003jd004169, 2004.

Price-Allison, A., Lea-Langton, A. R., Mitchell, E. J. S., Gudka, B., Jones, J. M., Mason, P. E., and Williams, A.: Emissions performance of high moisture wood fuels burned in a residential stove, Fuel, 239, 1038–1045, https://doi.org/10.1016/j.fuel.2018.11.090, 2019.

Price-Allison, A., Mason, P. E., Jones, J. M., Barimah, E. K., Jose, G., Brown, A. E., Ross, A. B., and Williams, A.: The Impact of Fuelwood Moisture Content on the Emission of Gaseous and Particulate Pollutants from a Wood Stove, Combust. Sci. Technol., 195, 133–152, https://doi.org/10.1080/00102202.2021.1938559, 2021.

Rathod, T. D. and Sahu, S. K.: Measurements of optical properties of black and brown carbon using multi-wavelength absorption technique at Mumbai, India, J. Earth Syst. Sci., 131, 32, https://doi.org/10.1007/s12040-021-01774-0, 2022.

Reda, A. A., Czech, H., Schnelle-Kreis, J., Sippula, O., Orasche, J., Weggler, B., Abbaszade, G., Arteaga-Salas, J. M., Kortelainen, M., Tissari, J., Jokiniemi, J., Streibel, T., and Zimmermann, R.: Analysis of gas-phase carbonyl compounds in emissions from modern wood combustion appliances: Influence of wood type and combustion appliance, Energ. Fuel., 29, 3897–3907, https://doi.org/10.1021/EF502877C, 2015.

Reid, J. S., Koppmann, R., Eck, T. F., and Eleuterio, D. P.: A review of biomass burning emissions part II: intensive physical properties of biomass burning particles, Atmos. Chem. Phys., 5, 799–825, https://doi.org/10.5194/acp-5-799-2005, 2005.

Romshoo, B., Müller, T., Pfeifer, S., Saturno, J., Nowak, A., Ciupek, K., Quincey, P., and Wiedensohler, A.: Optical properties of coated black carbon aggregates: numerical simulations, radiative forcing estimates, and size-resolved parameterization scheme, Atmos. Chem. Phys., 21, 12989–13010, https://doi.org/10.5194/acp-21-12989-2021, 2021.

Saleh, R., Hennigan, C. J., McMeeking, G. R., Chuang, W. K., Robinson, E. S., Coe, H., Donahue, N. M., and Robinson, A. L.: Absorptivity of brown carbon in fresh and photo-chemically aged biomass-burning emissions, Atmos. Chem. Phys., 13, 7683–7693, https://doi.org/10.5194/acp-13-7683-2013, 2013.

Saleh, R., Robinson, E. S., Tkacik, D. S., Ahern, A. T., Liu, S., Aiken, A. C., Sullivan, R. C., Presto, A. A., Dubey, M. K., Yokelson, R. J., Donahue, N. M., and Robinson, A. L.: Brownness of organics in aerosols from biomass burning linked to their black carbon content, Nat. Geosci., 7, 647–650, https://doi.org/10.1038/ngeo2220, 2014.

Saliba, G., Subramanian, R., Bilsback, K., L'Orange, C., Volckens, J., Johnson, M., and Robinson, A. L.: Aerosol Optical Properties and Climate Implications of Emissions from Traditional and Improved Cookstoves, Environ. Sci. Technol., 52, 13647–13656, https://doi.org/10.1021/acs.est.8b05434, 2018.

Sandradewi, J., Prévôt, A. S. H., Szidat, S., Perron, N., Alfarra, M. R., Lanz, V. A., Weingartner, E., and Baltensperger, U.: Using aerosol light absorption measurements for the quantitative determination of wood burning and traffic emission contribution to particulate matter, Environ. Sci. Technol., 42, 3316–3323, https://doi.org/10.1021/es702253m, 2008.

Savolahti, M., Karvosenoja, N., Tissari, J., Kupiainen, K., Sippula, O., and Jokiniemi, J.: Black carbon and fine particle emissions in Finnish residential wood combustion: Emission projections, reduction measures and the impact of combustion practices, Atmos. Environ., 140, 495–505, https://doi.org/10.1016/j.atmosenv.2016.06.023, 2016.

Savolahti, M., Karvosenoja, N., Soimakallio, S., Kupiainen, K., Tissari, J., and Paunu, V. V.: Near-term climate impacts of Finnish residential wood combustion, Energ. Policy, 133, 110837, https://doi.org/10.1016/J.ENPOL.2019.06.045, 2019.

Shen, G., Wang, W., Yang, Y., Ding, J., Xue, M., Min, Y., Zhu, C., Shen, H., Li, W., Wang, B., Wang, R., Wang, X., Tao, S., and Russell, A. G.: Emissions of PAHs from indoor crop residue burning in a typical rural stove: Emission factors, size distributions, and gas-particle partitioning, Environ. Sci. Technol., 45, 1206–1212, https://doi.org/10.1021/es102151w, 2011.

Sippula, O., Hokkinen, J., Puustinen, H., Yli-Pirilä, P., and Jokiniemi, J.: Particle emissions from small wood-fired district heating units, Energ. Fuel., 23, 2974–2982, https://doi.org/10.1021/ef900098v, 2009.

Suhonen, H., Laitinen, A., Kortelainen, M., Koponen, H., Kinnunen, N., Suvanto, M., Tissari, J., and Sippula, O.: Novel fine particle reduction method for wood stoves based on high-temperature electric collection of naturally charged soot particles, J. Clean. Prod., 312, 127831, https://doi.org/10.1016/J.JCLEPRO.2021.127831, 2021.

Sun, J., Zhang, Y., Zhi, G., Hitzenberger, R., Jin, W., Chen, Y., Wang, L., Tian, C., Li, Z., Chen, R., Xiao, W., Cheng, Y., Yang, W., Yao, L., Cao, Y., Huang, D., Qiu, Y., Xu, J., Xia, X., Yang, X., Zhang, X., Zong, Z., Song, Y., and Wu, C.: Brown carbon's emission factors and optical characteristics in household biomass burning: developing a novel algorithm for estimating the contribution of brown carbon, Atmos. Chem. Phys., 21, 2329–2341, https://doi.org/10.5194/acp-21-2329-2021, 2021.

Tasoglou, A., Saliba, G., Subramanian, R., and Pandis, S. N.: Absorption of chemically aged biomass burning carbonaceous aerosol, J. Aerosol Sci., 113, 141–152, https://doi.org/10.1016/J.JAEROSCI.2017.07.011, 2017.

Tian, J., Wang, Q., Ni, H., Wang, M., Zhou, Y., Han, Y., Shen, Z., Pongpiachan, S., Zhang, N., Zhao, Z., Zhang, Q., Zhang, Y., Long, X., and Cao, J.: Emission Characteristics of Primary Brown Carbon Absorption From Biomass and

Coal Burning: Development of an Optical Emission Inventory for China, J. Geophys. Res.-Atmos., 124, 1879–1893, https://doi.org/10.1029/2018JD029352, 2019.

Tian, P., Liu, D., Zhao, D., Yu, C., Liu, Q., Huang, M., Deng, Z., Ran, L., Wu, Y., Ding, S., Hu, K., Zhao, G., Zhao, C., and Ding, D.: In situ vertical characteristics of optical properties and heating rates of aerosol over Beijing, Atmos. Chem. Phys., 20, 2603–2622, https://doi.org/10.5194/acp-20-2603-2020, 2020.

Tissari, J., Väätäinen, S., Leskinen, J., Savolahti, M., Lamberg, H., Kortelainen, M., Karvosenoja, N., and Sippula, O.: Fine particle emissions from sauna stoves: Effects of combustion appliance and fuel, and implications for the Finnish emission inventory, Atmosphere, 10, 775, https://doi.org/10.3390/ATMOS10120775, 2019.

Turpin, B. J., Saxena, P., and Andrews, E.: Measuring and simulating particulate organics in the atmosphere: problems and prospects, Atmos. Environ., 34, 2983–3013, https://doi.org/10.1016/S1352-2310(99)00501-4, 2000.

Vicente, E. D. and Alves, C. A.: An overview of particulate emissions from residential biomass combustion, Atmos. Res., 199, 159–185, https://doi.org/10.1016/j.atmosres.2017.08.027, 2018.

Virkkula, A.: Modeled source apportionment of black carbon particles coated with a light-scattering shell, Atmos. Meas. Tech., 14, 3707–3719, https://doi.org/10.5194/amt-14-3707-2021, 2021.

Virkkula, A., Mäkelä, T., Hillamo, R., Yli-Tuomi, T., Hirsikko, A., Hämeri, K., and Koponen, I. K.: A simple procedure for correcting loading effects of aethalometer data, J. Air Waste Manag. Assoc., 57, 1214–1222, https://doi.org/10.3155/1047-3289.57.10.1214, 2007.

Wang, Q., Han, Y., Ye, J., Liu, S., Pongpiachan, S., Zhang, N., Han, Y., Tian, J., Wu, C., Long, X., Zhang, Q., Zhang, W., Zhao, Z., and Cao, J.: High Contribution of Secondary Brown Carbon to Aerosol Light Absorption in the Southeastern Margin of Tibetan Plateau, Geophys. Res. Lett., 46, 4962–4970, https://doi.org/10.1029/2019GL082731, 2019.

Weingartner, E., Saathoff, H., Schnaiter, M., Streit, N., Bitnar, B., and Baltensperger, U.: Absorption of light by soot particles: Determination of the absorption coefficient by means of aethalometers, J. Aerosol Sci., 34, 1445–1463, https://doi.org/10.1016/S0021-8502(03)00359-8, 2003.

Wu, B., Xuan, K., Zhang, X., Shen, X., Li, X., Zhou, Q., Cao, X., Zhang, H., and Yao, Z.: Mass absorption cross-section of black carbon from residential biofuel stoves and diesel trucks based on real-world measurements, Sci. Total Environ., 784, 147225, https://doi.org/10.1016/J.SCITOTENV.2021.147225, 2021.

Wu, C., Huang, X. H. H., Ng, W. M., Griffith, S. M., and Yu, J. Z.: Inter-comparison of NIOSH and IMPROVE protocols for OC and EC determination: implications for inter-protocol data conversion, Atmos. Meas. Tech., 9, 4547–4560, https://doi.org/10.5194/amt-9-4547-2016, 2016.

Yang, J., Au, W. C., Law, H., Lam, C. H., and Nah, T.: Formation and evolution of brown carbon during aqueous-phase nitrate-mediated photooxidation of guaiacol and 5-nitroguaiacol, Atmos. Environ., 254, 118401, https://doi.org/10.1016/J.ATMOSENV.2021.118401, 2021.

Yus-Díez, J., Bernardoni, V., Močnik, G., Alastuey, A., Ciniglia, D., Ivančič, M., Querol, X., Perez, N., Reche, C., Rigler, M., Vecchi, R., Valentini, S., and Pandolfi, M.: Determination of the multiple-scattering correction factor and its cross-sensitivity to scattering and wavelength dependence for different AE33 Aethalometer filter tapes: a multi-instrumental approach, Atmos. Meas. Tech., 14, 6335–6355, https://doi.org/10.5194/amt-14-6335-2021, 2021.

Zhang, G., Peng, L., Lian, X., Lin, Q., Bi, X., Chen, D., Li, M., Li, L., Wang, X., and Sheng, G.: An improved absorption Ångström exponent (AAE)-based method for evaluating the contribution of light absorption from brown carbon with a high-time resolution, Aerosol Air Qual. Res., 19, 15–24, https://doi.org/10.4209/aaqr.2017.12.0566, 2019.

Zhang, L., Luo, Z., Du, W., Li, G., Shen, G., Cheng, H., and Tao, S.: Light absorption properties and absorption emission factors for indoor biomass burning, Environ. Pollut., 267, 115652, https://doi.org/10.1016/j.envpol.2020.115652, 2020.

Zhang, L., Luo, Z., Li, Y., Chen, Y., Du, W., Li, G., Cheng, H., Shen, G., and Tao, S.: Optically Measured Black and Particulate Brown Carbon Emission Factors from Real-World Residential Combustion Predominantly Affected by Fuel Differences, Environ. Sci. Technol., 55, 169–178, https://doi.org/10.1021/ACS.EST.0C04784, 2021.

Zhong, M. and Jang, M.: Dynamic light absorption of biomass-burning organic carbon photochemically aged under natural sunlight, Atmos. Chem. Phys., 14, 1517–1525, https://doi.org/10.5194/acp-14-1517-2014, 2014.

Zotter, P., Herich, H., Gysel, M., El-Haddad, I., Zhang, Y., Močnik, G., Hüglin, C., Baltensperger, U., Szidat, S., and Prévôt, A. S. H.: Evaluation of the absorption Ångström exponents for traffic and wood burning in the Aethalometer-based source apportionment using radiocarbon measurements of ambient aerosol, Atmos. Chem. Phys., 17, 4229–4249, https://doi.org/10.5194/acp-17-4229-2017, 2017.